Brain Mechanisms Underlying Integration of Optic Flow and Vestibular Cues to Self-motion

Maiko Uesaki

Abstract

Optic flow is a retinal motion pattern that occurs as the observer moves through an environment. Optic flow provides the observer with information necessary for accurately estimating the observer's position, orientation and displacement with regard to the environment, and is therefore one of the most important sensory cues to perception of self-motion.

A network of cortical sensory areas that underlie the processing of optic flow has been identified in the recent functional neuroimaging studies. These optic-flow selective areas include the middle temporal complex (MT+), V6 in the parieto-occipital sulcus, the ventral intraparietal area (VIP), the putative area 2v (p2v), the cingulate sulcus visual area (CSv) and the region of the precuneus dorsal to the ascending arm of the cingulate sulcus (precuneus motion area; PcM), the posterior-insular complex (PIC+). However, few studies have investigated the roles of and interaction between the optic-flow selective areas in visuo-vestibular integration necessary for the accurate perception of self-motion. Since coherent perception of self-motion is constructed by integrating sensory information, including visual and vestibular signals, Chapter 2 aimed to identify optic-flow selective areas that are the loci in visuo-vestibular integration necessary for optic-flow processing and therefore accurate perception of self-motion. Under certain circumstances, optic flow can induce an illusory sensation of self-motion (i.e. vection). The study described in Chapter 2 investigated whether the optic-flow stimulus was encoded differently in the optic-flow selective areas depending on the presence or absence of the sensation of self-motion, by introducing vection as an index, using functional magnetic resonance imaging (fMRI) in conjunction with behavioural measurement. Results showed that activity in visual areas MT+ and V6, polysensory areas VIP and PIC+ was significantly greater while subjects were experiencing vection, as compared to

when they were experiencing no sensation of self-motion. The findings place polysensory areas VIP and PIC+ in a good position to integrate visual cues to self-motion and vestibular information (or lack thereof).

Whilst Chapter 2 emphasises the functional aspect of the anatomical mechanism underlying visuo-vestibular integration involved in the processing of optic flow, Chapter 3 focuses on the structural aspect of the mechanism. Chapter 2 revealed that VIP located in the superior part of the parietal cortex and PIC+ in the inferior part of the parietal cortex are the loci of visuo-vestibular integration necessary for accurate perception of optic flow, but these areas are few centimetres apart in the brain. Chapter 3 aimed to investigate how these distant areas communicate through the white matter, by employing a combination of fMRI, diffusion-weighted magnetic resonance imaging (dMRI) and tractography. Recent advances in dMRI and tractography have enabled identification and characterisation of major long-range white matter tract in the living human brain. Yet, our understanding of shorter tracts, such as those within the parietal cortex, remains limited. Over a century ago, a tract connecting the superior and inferior parts of the parietal cortex was identified in a post-mortem study: *Stratum proprium of interparietal sulcus* (SIPS). The tract has since been replicated in another fibre dissection study, however, it has not been fully investigated in the living human brain and its precise anatomical properties are yet to be described. The study described in Chapter 3 used dMRI and tractography to identify and characterise SIPS in vivo, and explored its spatial proximity to optic-flow selective areas using fMRI. SIPS was identified bilaterally in all subjects, and its anatomical position and trajectory are consistent with previous post-mortem studies. Subsequent evaluation of the tractography results using the linear fascicle evaluation and virtual lesion analysis yielded strong statistical evidence for SIPS. The SIPS endpoints were found to be adjacent to the optic-flow selective areas. The findings show that SIPS is a short-range tract connecting the superior and inferior parts of the parietal cortex, wrapping

around the intraparietal sulcus, and that it may be a crucial anatomy underlying visuo-vestibular integration necessary for optic-flow processing.

Taken together, this thesis provides empirical evidence that polysensory areas VIP and PIC+ in the parietal cortex are the most likely candidates for areas whose interaction underlies the convergence of optic flow and vestibular cues to self-motion, and that these distant optic-flow selective areas probably transmit sensory information through SIPS. Thus, this thesis contributes to the literature of the brain mechanisms underlying visuo-vestibular integration necessary for perception of self-motion.

.

Contents

List of abbreviations

3D	Three dimensional
AF	Arcuate fasciculus
APCP	Anterior to posterior commissure
BOLD	Blood-oxygen-level-dependent
CingS	Cingulate sulcus
CS	Central sulcus
CSD	Constrained spherical deconvolution
CSv	Cingulate sulcus visual area
dMRI	Diffusion-weighted magnetic resonance imaging
EPI	Echo-planner imaging
ETC	Ensemble tractography connectome
fMRI	Functional magnetic resonance imaging
FA	Fractional anisotropy
FOD	Fibre orientation distribution
FoV	Field of view
GLM	General linear model
HCP	Human Connectome Project
ISI	Inter-stimulus interval
IPS	Intraparietal sulcus
KU	Kyoto University
LCD	Liquid crystal display
LiFE	Linear fascicle evaluation

LS	Lateral sulcus
LV	Lateral ventricle
MGH-USC HCP	Human Connectome Project by MGH-USC Consortium
MNI152	Montreal Neurological Institute 152
MP-RAGE	Magnetisation-prepared rapid-acquisition gradient echo
MR	Magnetic resonance
MRI	Magnetic resonance imaging
MST	Medial superior temporal area
MT+	Medial temporal complex
MVPA	Multi-voxel pattern analysis
NODDI	Neurite orientation dispersion and density imaging
p2v	Putative area 2v
pArc	Posterior arcuate
PcM	Precuneus motion area
PDD	Principal diffusion direction
PIC+	posterior insular complex
PIVC	Parieto-insular vestibular cortex
PoCS	Postcentral sulcus
RMSE	Root mean squared error
ROI	Region of interest
R_{rmse}	Ratio of root mean squared error
S	Strength of evidence
SD	Standard deviation
SIPS	Stratum proprium of interparietal sulcus
STS	Superior temporal sulcus

TE	Time echo
TR	Time of repetition
VOF	Vertical occipital fasciculus
WU-Minn HCP	Human Connectome Project by WU-Minn Consortium

Acknowledgements

I would like to thank all of those at School of Psychology, Graduate School of Letters, Kyoto University, past and present. The faculty members Hiroshi Ashida, Shoji Itakura, Kazuo Fujita and Yoshio Sakurai gave me advice on my research. The school administrator Tomomi Yokoyama made sure that I completed the necessary paperwork correctly and in time. Peers alongside whom I worked kept me going; especially Jasmina Stevanov and Benoit Bucher who are also great friends, let me bounce ideas and theories off of them and engaged in discussion about my research regardless of how unrelated it was to their own, whenever I got stuck.

I have been very fortunate to be surrounded by researchers who were always happy to offer support and guidance over the years. The members of the Japan Vision Society have provided me with feedback that improved my research. Michael Scheel at Charite Hospital (Berlin, Germany) and Wandell Lab in Psychology Department of Stanford University (California, USA) kindly hosted me as a visiting student and offered me the opportunity to gain the experience and skills necessary for the diffusion-weighted MRI study. I am particularly grateful to Hiromasa Takemura, who has provided me with not only technical guidance but also helped me with any challenges I faced as PhD student.

No one has taken more interest in or had more influence on my work than my supervisor Hiroshi Ashida. Despite my character flaws, he endorsed projects that were seemingly beyond my ability at the time, and always stood behind my choices. He carefully and sometimes strategically cultivated my interest in research and science, taught me not only about research in psychology and neuroscience, but also about ethics in science and in life. Had it not been for

his support, encouragement and extraordinary patience, I would not have been able to complete my PhD, let alone chosen to pursue a career in academia.

Thank you to my examiners, Christian Altmann, James Anderson, Hiroshi Ashida and Shoji Itakura for their time.

I would also like to mention Kokoro Research Center, Kyoto University and Japan Society for the Promotion of Science (JSPS). Both studies included in this thesis were conducted using the MRI scanner and related facilities of Kokoro Research Center, Kyoto University; and were partly supported by JSPS, Grant-in-Aid for JSPS Fellows.

To my family and AP: Thank you for the unconditional support and encouragement.

Author's declaration

I, Maiko Uesaki, declare that this thesis is a presentation of original work and I am the sole author. This work has not previously been presented for an award at this, or any other, University. All sources are acknowledged as References.

The empirical work presented in this thesis has been published in the following peer-reviewed journals, and the literature review is currently in preparation for submission:

Literature review bound in Chapter 1:

「自己運動に伴う感覚統合の神経基盤」in preparation for submission

Article bound in Chapter 2:

Optic-flow selective cortical sensory regions associated with self-reported states of vection. Uesaki M. & Ashida H. (2015). Frontiers in Psychology, 6:775.

Article bound in Chapter 3:

Computational neuroanatomy of human stratum proprium of interparietal sulcus. Uesaki M., Takemura H. & Ashida H. (2018). Brain Structure and Function, 223:489.

Results from the empirical chapters have been presented at the following conferences:

International conferences

Uesaki, M. Takemura, H. & Ashida, H. White-matter pathway connecting sensory cortical regions involved in optic-flow processing. *European Conference on Visual Perception 2015*. Liverpool, UK. 26 August 2015.

Uesaki, M. & Ashida, H. Neuronal representation of optic flow as a cue to self-motion. *The 16th International Multisensory Research Forum*. Pisa, Italy. June 2015.

Uesaki, M. & Ashida, H. Vection: Neuronal representation of optic flow as a cue to self-motion. *European Conference on Visual Perception 2014*, 32.20. Belgrade, Serbia. August 2014.

Uesaki, M. & Ashida, H. Connectivity between brain regions associated with optic-flow processing. *The 10th Asia-Pacific Conference on Vision*, 32.20. Takamatsu, Japan. July 2014.

Uesaki, M. & Ashida, H. Representation of egomotion in the brain and its relation to vection. *European Conference on Visual Perception 2012*, 65. Sardegna, Italy. September 2012.

Domestic conferences and workshops

上﨑麻衣子．オプティックフロー処理と視覚性自己運動感覚に関連する大脳皮質領野．東北大学電気通信研究所共同プロジェクト研究会「多感覚統合への自己身体運動の寄与」，仙台．2015 年 2 月．

上﨑麻衣子．オプティックフロー処理と視覚性自己運動感覚に関連する大脳皮質領野．東北大学電気通信研究所共同プロジェクト研究会「自己身体の運動が関与する多感覚統合」，仙台．2013 年 1 月．

上﨑麻衣子・竹村浩昌・蘆田宏．オプティックフロー選択性脳領域を結ぶ白質繊．日本視覚学会 2015 年冬季大会，3o02．東京．2015 年 1 月．ベスト・プレゼンテーション賞受賞

上﨑麻衣子・蘆田宏．視覚誘導性自己運動感覚の脳内表象．日本視覚学会 2012 年夏期季大会，8p10．山形．2012 年 8 月．

上﨑麻衣子・蘆田宏．オプティックフローに応答する大脳領野の定位．日本視覚学会 2012 年冬季大会，1p07．東京．2012 年 1 月．

Brain Mechanisms Underlying Integration of Optic Flow and Vestibular Cues to Self-motion

"If the human brain was so simple that we could understand it, we would be so simple that we couldn't"

---- Emerson M. Pugh

Chapter 1: Introduction

1. What is optic flow?

The complex motion pattern that is projected onto the retina as an observer moves through a structured environment is referred to as "optic flow" (Gibson 1950, 1954).

Mathematically, optic flow can be decomposed into three orthogonal vector fields, each of which indicates the direction and velocity of the local shift in the retinal image. One of the three pairs of vector field corresponds to spiral space (i.e. expansion/contraction and rotation; Graziano et al. 1994; Heuer & Britten 2007; Meese & Anderson 2002; Morrone et al. 1999; Snowden & Milne 1996), which provides information about the observer's position within, and relation to the environment (i.e. self-motion). Another corresponds to deformation space (Holliday & Meese 2008), which provides information about the structure of the environment. Points within spiral and deformation spaces represent uniform distributions of all local directions. The third component can be described in terms of translation space (Koenderink 1986; Koenderink & van Doorn 1975; Longuet-Higgins & Pranzdny 1980), a point within which represents a single direction of uniform motion.

Optic flow provides the observer with information such as direction of heading (Gibson 1950, 1954; Lappe et al. 1999; Warren & Hannon 1988; Furlan et al. 2013), time to contact (Lee 1980), distance travelled (Redlick et al. 2001), segmentation of object motion (Logan & Duffy 2006; Warren & Rushton 2008), and the slant of surfaces in the scene (Koenderink 1986).

2. Cortical mechanisms of optic-flow processing

Human sensory systems effectively utilise such information to accurately estimate the observer's position, orientation and displacement, which support safe and successful navigation through the given environment. For example, observers can identify the focus of expansion (Bex & Falkenberg 2006; Warren & Hannon 1988) and make accurate judgements of their heading based on this (Crowell & Banks 1993), even in the presence of head as well as eye movements (Royden et al. 1992; Royden & Picone 2007). A global analysis of the expansion component in optic flow is used to calculate time-to-contact (Giachritsis & Harris 2005), rotation is used to compensate retinal flow for observer roll (Hanada & Ejima 2000), expansion and rotation are used to control posture (Lee & Aronson 1974), and deforming flow structures give a sense of the slant of the moving surfaces of the environment (Domini & Caudek 1999; Freeman et al. 1996; Meese & Harris 1997; Meese et al. 1995; Zhong et al. 2006).

Visual areas

Evidence that primate vision contains the appropriate specialised mechanisms to perform these analyses comes from psychophysics (Bex et al. 1998, 1999; Burr & Santoro 2001; Freeman & Harris 1992; Gurney & Wright 1996; Meese & Harris 2001a, 2001b; Morrone et al. 1995; Snowden & Milne 1996, 1997), single-cell recordings (Duffy & Wurtz 1991a, 1991b; Saito et al. 1986; Tanaka & Saito 1989), and functional imaging (Dupont et al. 1994; Goossens et al. 2006; Morrone et al. 2000; Smith et al. 2006; Wall & Smith 2008; Cardin & Smith 2010, 2011; Pitzalis et al. 2010; Furlan et al. 2013).

Earlier studies shed light on an extensive network of motion sensitive areas in the parietally directed stream of the visual cortex, both within and beyond the well-established middle temporal (MT) cortical area (Annese et al. 2005; Dumoulin et al. 2000; van Essen et al. 1981). The cortex in the proximity of the classically defined MT area is subdivided into several nodes supporting different aspects of motion analysis (Huk et al. 2002; Matsumoto et al. 2004). This larger area is often referred to as MT complex (MT+) to reflect this fact.

In addition to the MT+, there are many reports of motion processing outside this area. One area that has recently been identified is V6 in the parieto-occipital sulcus. Like MT+, V6 has been shown to responds differentially to coherent optic flow (Dukelow et al. 2001; Morrone et al. 2000; Wall & Smith 2008; Cardin & Smith 2010, 2011; Pitzalis et al. 2010), particularly, when it is relevant for self-motion (Furlan et al. 2013).

Polysensory areas in the parietal cortex

Evidence is also accumulating of the involvement of polysensory areas in the parietal cortex, in higher order motion processing. Although for humans, as well as for many other species, vision dominates over other senses, under certain circumstances visual system alone cannot provide reliable input. For this reason, human sensory system relies on a multitude of different sensory inputs such as visual and vestibular cues, which allows for a more precise estimate of self-motion (Alais & Burr 2004; Butler et al. 2010; Ernst & Banks 2002; Knill & Saunders 2003). When the sensory systems receive inputs during self-motion, these inputs are evaluated, weighted and integrated according to their reliability (Fetsch et al. 2012). This sensory integration indicates the involvement of polysensory areas. Beyond the visual cortex along the parietally directed stream, lies the ventral intraparietal area (VIP; Felleman & van Essen 1991; Andersen et al. 1990). In primates, it has long been known that along with MT+, VIP contains

neurons that are selectively sensitive to optic flow (Tanaka & Saito 1989; Duffy & Wurts 1991; Schaafsma & Duysens 1996). Many neurons in VIP are polysensory, and respond to not only visual but also receives vestibular input (Gu et al. 2006; Chen et al. 2011; Fetsch et al. 2012; Duhamel et al. 1998; Bremmer et al. 2001; Lewis & van Essen 2000; Cottereau et al. 2017). In the human brain, VIP has also been shown to be involved in encoding optic flow (Wall & Smith 2008; Cardin & Smith 2010, 2011). Slightly anterior to VIP, in the junction of the intraparietal sulcus, there is the putative area 2v (p2v) that is known to be primarily vestibular but also receives visual and proprioceptive information (Guldin & Grusser 1998) and responds selectively to optic flow (Cardin & Smith 2010, 2011).

Medially, areas such as the cingulate sulcus visual area (CSv) and the region of the precuneus dorsal to the ascending arm of the cingulate sulcus (precuneus motion area; PcM) have recently been shown to have selectivity to optic-flow stimulation. CSv had not previously been associated with optic-flow processing and is not located in the cingulate, but recent studies confirm the role of CSv in visual self-motion processing in humans (Antal et al. 2008; Fischer et al. 2012; Wall & Smith 2008; Smith et al. 2012) as well as in macaques (Cottereau et al. 2017). PcM was first described by Cardin & Smith (2010; although included in one of the larger areas identified in Kovacs et al. 2008) as an area selective for coherent flow patterns (Wada et al. 2016).

An area in the inferior part of the parietal cortex has also been implicated in optic-flow processing. Initially (and probably wrongly; for review, see Greenlee et al. 2016) labelled the parieto-insular vestibular cortex (PIVC) in a few imaging studies, the posterior-insular complex (PIC+: Deutschländer et al. 2004; Cardin & Smith 2010, 2011; Biagi et al. 2015; Uesaki & Ashida 2015; Wada et al. 2016) has repeatedly been shown to respond selectively to optic flow.

PIC+ is located immediately posterior to PIVC, and is a visual-vestibular area (Frank et al. 2014; Frank et al. 2016; Greenlee et al. 2016).

Such evidence is testament to the fact that coherent perception of self-motion is constructed by integrating sensory information, including visual and vestibular signals (Wertheim 1994; Wexler et al. 2001).

3. White matter anatomy

Since a vast network comprised of distant cortical areas underlies the accurate calculation of optic flow, investigation of the white matter structure that allows transmission of information amongst those areas seems in order for a more comprehensive understanding of the anatomical mechanisms for optic-flow processing.

Anatomical connections through the white matter axon bundles (i.e. fascicles, tracts) establish fundamental features of the brain's information processing (Catani & Ffytche 2005; Catani & Thiebaut de Schotten 2012; Bullock et al. 2005; Fields 2008, 2015; Wandell & Yeatman 2013; Wandell 2005). Diffusion-weighted magnetic resonance imaging (dMRI) and tractography provide a unique opportunity to identify and characterise the white matter tracts in the living human brain (Catani et al. 2002; Wakana et al. 2004; Mori & Zhang 2006; Catani & Thiebaut de Schotten 2012; Craddock et al. 2013; Wandell 2016; Rokem et al. 2017).

A body of dMRI research has successfully identified several major long-range white matter tracts, such as the superior longitudinal fasciculus and the inferior longitudinal fasciculus, in a

consistent manner with the known post-mortem anatomy (Catani et al. 2002; Wakana et al. 2004; Schmahmann et al. 2007), and ergo opened new avenues to research on the property of major human white matter tracts in relation to development and diseases (Lebel et al. 2012; Yeatman, Dougherty, Ben-Shachar et al. 2012; Ogawa et al. 2014; Yeatman, Wandell et al. 2014; Malania et al., 2017). More recent dMRI studies have identified shorter white matter tracts including frontal aslant tract and vertical occipital fasciculus, which, partially for their relatively short trajectories, had previously received very little attention in the neuroscience literature (Thiebaut de Schotten et al. 2012; Catani et al. 2012; Catani et al. 2013; Yeatman et al. 2013; Yeatman, Weiner et al. 2014; Takemura, Rokem et al. 2016). Some of those studies have suggested the importance of the shorter tracts in relation to cognitive functions and diseases (Kinoshita et al. 2015; Kemerdere et al. 2016; Kronfeld-Duenias et al. 2016; Duan et al. 2015; Takemura, Rokem et al. 2016; Lee Masson et al. 2017).

Because the technology that enables non-invasive studies of the white matter anatomy in the living human brain has only recently become available, there has not been much research on the white matter structure connecting the optic-flow selective areas in the human brain.

One very recent study by Smith and colleagues (2017) has investigated the white matter connectivity pattern of CSv using dMRI in conjunction with resting-state functional magnetic resonance imaging (fMRI). The study found that CSv is statistically likely to be connected to other optic-flow selective areas such as V6, VIP and PIC+. The white matter connections amongst the other optic-flow selective areas remain unknown.

4. Thesis overview: What does this thesis aim to address?

My research interests lie in anatomical mechanisms for processing optic flow: In particular, optic flow as a cue to self-motion.

The articles referenced in this thesis addressed the following questions:

1. Which of the areas responsive to optic flow are pivotal in sensory integration underlying self-motion perception?
2. How do those distant areas channel sensory signals to each other?

Advances in neuroimaging technology over the past three decades have opened new avenues to non-invasively studying the living human brain. The accessibility to increasingly sophisticated and affordable equipment has enabled a multimodal approach.

Depending on the question to be answered, there are advantages as well as disadvantages to certain techniques over others. For example, fMRI along with positron emission tomography and functional near-infrared spectroscopy provide more precise information regarding locations of sources of brain activity, but their limited temporal resolution means they can only provide a very course estimate of the temporal evolution of cortical processing across a network of brain areas. Conversely, electroencephalography/magnetoencephalography allows for directionality of the spread of activation across a network of brain areas with higher temporal precision, at a cost of the spatial arrangement of the areas within that network. Structural MRI techniques including diffusion-weighted MRI can be used to investigate the likely structural routes of information transmission between areas in the brain network.

The same principle applies to the methods of analysis. Just like for the imaging techniques, there are advantages and disadvantages to a certain analytical method over others.

With this in mind, my approach to addressing these questions, with relevant publications, is broken down as follows in the main body of this thesis:

Chapter 2: Differential encoding of optic-flow reveals the loci of visuo-vestibular integration during perception of self-motion

In this section of the thesis, I describe the study aimed to identify optic-flow selective sensory areas that are involved in the processing of visual cues to self-motion, by introducing an illusory sensation of self-motion as an index and assessing activation in which of those areas reflect the sensation of self-motion, using fMRI. FMRI has become one of the most commonly used method for measuring neural responses in the living brain. As the firing rate of neurons increase, those neurons consume their energy reserves which then need to be replenished. This process requires an increase in the transfer of oxygen to those cells via the bloodstream, which causes a local change in the proportion of oxygenated haemoglobin in the blood. The MRI contrast termed blood oxygenation level-dependent (BOLD; Ogawa et al. 1990) provides a measure of this oxygenation change. Vascular changes in the brain indicated by the BOLD signals can be used to infer the underlying neural activity. In *Optic-flow selective cortical sensory regions associated with self-reported states of vection*, the combination of fMRI and behavioural measurements gave novel insights into the differential encoding of optic flow depending on the presence/absence of the sensation of self-motion. In particular, the polysensory areas VIP and PIC+ in the parietal cortex were found to be the loci of visuo-

vestibular integration. The findings also indicated that activity in the optic-flow selective visual areas MT+ and V6 was modulated by the feedback from those polysensory areas.

Chapter 3: Stratum proprium of interparietal sulcus supports communication between optic-flow selective areas involved in visuo-vestibular integration

Since we identified the optic-flow selective areas that integrate visual and vestibular cues to self-motion, we were interested in finding out how those distant areas were connected through the white matter. The white matter mainly composed of myelinated axons, also referred to as tracts, that coordinate communication between different brain areas. Bundles of the axons constitute the structure that restricts the rate of local mobility of water molecules, which can be estimated from dMRI data. Computing the diffusion within each image voxel based on dMRI data allows for reconstruction of streamlines, which are then used to estimate the tracts within the white matter. This modelling technique is referred to as tractography (Basser et al. 2000). In *Computational neuroanatomy of human proprium stratum of interparietal sulcus*, we combined fMRI, dMRI and tractography to investigate the white matter tract that connects the optic-flow selective areas in the superior and inferior parts of the parietal cortex, underlying the visuo-vestibular integration necessary for perception of optic flow and self-motion.

How do our publications form a coherent body of work?

The study described in Chapter 2 examined the activity of the previously identified optic-flow selective areas during reported states of illusory self-motion, and showed that polysensory areas in the superior and inferior parietal cortices play a critical role in visuo-vestibular integration underlying perception of optic flow as a cue to self-motion. In Chapter 3, we

identified and characterised the white matter tract that connects the superior and inferior parietal cortices. The work as a whole aims to provide a comprehensive view of the anatomical mechanisms underlying multisensory integration required for accurate perception of optic flow and self-motion. The research is therefore highly related and forms a coherent body of work.

Chapter 2: Differential encoding of optic flow reveals the loci of visuo-vestibular integration during perception of self-motion

1. Introduction

Optic flow is the pattern of apparent motion on the retina caused by the relative motion between an observer and the scene, and is one of the most important visual cue for the estimation of self-motion (Gibson 1950, 1954; Warren et al. 1988).

It has been shown that there is a network of cortical sensory areas that respond selectively to optic flow (Duffy & Wurts 1991a, 1991b, 1995; Cardin & Smith 2010, 2011). Those areas are; the middle temporal cortex (MT+), V6, the ventral intra-parietal area (VIP), cingulate sulcus visual area (CSv), precuneus motion area (PcM), putative area 2v (p2v) and the posterior insular complex (PIC+).

Although generally, perception of self-motion depends on inputs from a multitude of sensory systems (Howard & Templeton 1966), there are circumstances under which available sensory

information is restricted. When visual information (i.e. optic flow) is the sole cue to computing self-motion parameters, the discrepancy amongst the sensory signals may arise and as a result, induce an illusion of self-motion (Dichgans & Brandt 1978). For example, when we sit on a stationary train in the station and the train in the next platform starts moving, many of us experience the sensation that the train we are sitting on has started moving. This visually induced sensation of self-motion is referred to as 'vection' (Brandt et al. 1972; Koenderink 1986; Lappe et al. 1999). By introducing vection as an index, it might be possible to identify cortical sensory areas that are involved in integration of visual information related to self-motion and vestibular information (or lack thereof).

Kovacs et al. (2008) investigated cortical areas, of which activation is correlated with vection. In their study, subjects passively viewed two types of optic-flow stimulus: One was perceived predominantly as a cue to self-motion and the other perceived predominantly as a cue to object-motion. By contrasting the cortical activation patterns during subjects' observation of the two types of optic-flow stimulus, they found that MT+, precuneus, an area corresponding to VIP in the right hemisphere, and areas corresponding to V6 and CSv in the left hemisphere. These findings are partially corroborated by Wall and Smith (2008) that suggests that areas MST, MT, CSv and VIP exhibit differential responses to optic-flow stimuli that are compatible with self-motion.

A polysensory area PIC+ immediately posterior to the area corresponding to monkey parieto-insular vestibular cortex (PIVC) has also been implicated in the cortical representation of vection: Brandt et al. (1998), Deutschlander et al. (2004) and Kleinschmidt et al. (2002) reported deactivation in posterior insular cortex while subjects were experiencing vection.

Many of the cortical sensory areas that respond selectively to optic flow (Cardin & Smith 2010, 2011) have been associated with vection. However, few studies have investigated the roles of and interaction between the optic-flow selective sensory areas in visuo-vestibular integration underlying the accurate perception of optic flow as well as self-motion, by functionally identifying those areas prior to the experiment, and directly correlating activation in those areas and presence of vection using a regions-of-interest (ROI) analysis. Consequently, the cortical sensory areas that are involved in integration of visual information related to self-motion and vestibular information are yet to be identified.

This study aimed to determine which of the optic-flow selective sensory areas are the loci of integration of optic flow and vestibular information related to self-motion, by assessing whether optic flow is encoded differently according to the presence or absence of vection, and if so, activation in which of those areas reflect vection, using functional magnetic resonance imaging (fMRI).

2. Methods

2.1. Subjects

Three healthy volunteers (two males and one female; of the ages between 25 and 47 years) participated in the study. All had normal or corrected-to-normal vision and were screened according to standard MRI exclusion criteria. Subjects gave written informed consent to take part in this study, which was conducted in accordance with the ethical standards stated in the

Declaration of Helsinki and approved by the local ethics and safety committees at Kyoto University.

2.2. Data acquisition

MR images were obtained with a 3-Tesla Siemens Magnetom Verio scanner (Siemens, Erlangen, Germany) and a Siemens 32-channel posterior-head array coil that gives improved signal-to-noise ratio in the occipital cortex at the expense of the anterior part of the brain. For each subject, a high-resolution T1-weighted 3D anatomical image was acquired (magnetisation-prepared rapid-acquisition gradient echo (MP-RAGE), Siemens; 208 axial slices, 1-mm isotropic voxels, time of repetition (TR) = 2250 ms, time echo (TE) = 3.51 ms, field of view (FoV) = 256 x 256 mm^2, flip angle = 9°, bandwidth = 230 Hz/pixel). This anatomical image was used as a reference to which the functional images were coregistered. The functional data were acquired with a gradient echo, echo-planner sequence (39 contiguous axial slices, 3-mm isotropic voxels, TR = 2000 ms, TE = 25 ms, FoV = 192 x 192 mm^2, flip angle = 80°, bandwidth = 2368 Hz/pixel). Each experimental run lasted 4 min 16 s for both the main experiment and the localiser. For coregistration purposes (see Data analysis), between the functional and anatomical scans, a single-volume echo-planner imaging (EPI) sequence was acquired with the same position parameters as in the experimental runs.

2.3. Stimuli and procedure

Stimuli for both the main experiment and the localiser were displayed onto an in-bore rear-projection screen in the MRI machine by means of a liquid crystal display (LCD) projector, viewed via MaxTV binocular magnifier goggles (Eschenbach Optik GmbH, Nuremberg,

Germany; the metal parts were removed) in order to maximise the stimulated area of the visual field. The images subtended 30 x 30 degree visual angle and had a resolution of 768 x 768 pixels with a refresh rate of 60 Hz. The stimulus for the main experiment was a random dot kinematogram consisting of 200 moving white square dots of 10 x 10 pixels (subtending approximately 0.4 x 0.4 degree visual angle), on a dark background. The dots, which initially appeared at random locations, formed a circular patch of 30-degree diameter. Motion directions of the dots were arranged so that the dots cycled through a spiral space with time-varying trajectories away from and towards the centre of the patch. The trajectories were defined by the equations proposed in Morrone et al. (2000):

$$dr/dt = r\ v \cos\ \phi \qquad [1]$$
$$d\theta/dt = v \sin\ \phi$$

or

$$dr/dt = r\ v \cos\ \phi \qquad [2]$$
$$d\theta/dt = (v \sin\ \phi)/r,$$

where (r, θ) corresponds to the position in the polar coordinates ($0 \leq r \leq 1$), ϕ determines the spiral direction of flow and v is the dot speed. ϕ was linearly increased at the rate of 0.25π/s (i.e. 8 s/cycle). Expansion and contraction simulated forward and backwards motion of the observer, respectively.

Although the average speed of the dots was maintained at 3.54 pixel/frame (~= 8.3 deg/s) throughout the experiment, the speed gradient was manipulated to create two conditions:

Gradient condition and no-gradient condition. In the gradient condition (equation [1]), the speed of the dots increased linearly with eccentricity in all directions from the centre (minimum: 0.625 pixels/frame ~= 1.5 deg/s; maximum: 5 pixels/frame ~= 11.7 deg/s). Dots near the centre of the display moved slower whilst dots in the periphery moved faster, which made the pattern consistent with optic flow on the retina during self-motion in terms of speed. In the no gradient condition (equation [2]), no speed gradient was applied to the motion of the dots, i.e., the speed at which the dots moved was constant at all locations in the display, which is inconsistent with optic flow during self-motion.

These two conditions were presented in a block design in a back-to-back manner (i.e. gradient–no-gradient–no-gradient–gradient–gradient and so on; Figure 1). Within each block, one of the two types of optic-flow stimulus was presented for 16 s, followed by a 16-s inter-stimulus interval (ISI); and within each experimental run, there were eight stimulus blocks (four blocks per condition). Subjects took part in 10 experimental runs (over two scans conducted on two non-consecutive days), each lasting 4 min 16 s.

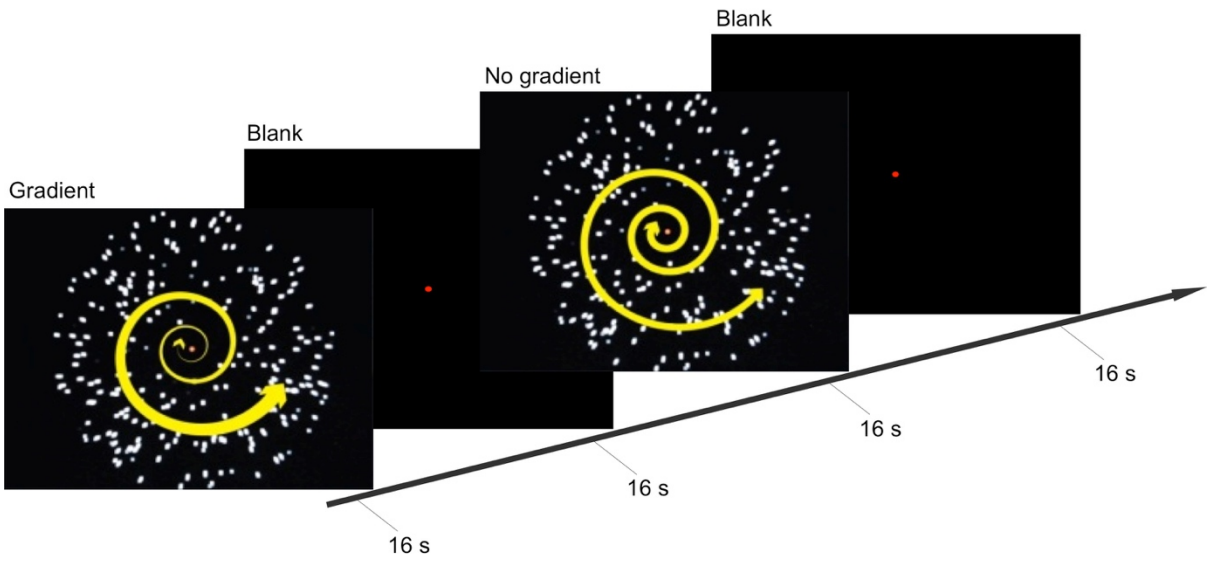

Figure 1. Experimental procedure and stimuli. Timeline illustrates the stimuli presented during the gradient and no-gradient conditions, and a blank screen with a fixation point presented during ISI. During the stimulus-presentation blocks, subjects held down one of the two buttons to indicate whether they were experiencing vection or no vection.

The experiment also employed an event-related design to allow for a more direct inference on correlation between the observed cortical activity and vection. During the stimulus-presentation phase of each block, subjects pressed one of the two buttons to indicate whether or not they were experiencing vection. Pressing one of the two buttons indicated the onset of vection, the other indicated the onset of visual stimulation that was not accompanied by vection or the offset of vection. Consequently, a sequence of alternating button presses was recorded, identifying periods of time during which subjects perceived themselves to be moving (vection) and to be stationary (no vection).

A red central fixation point was provided throughout the experimental runs, and subjects were instructed to maintain fixation at all times.

2.4. Functional localiser

In order to quantify activity during the main experiment, various regions of interest (ROIs) previously associated with optic-flow processing or self-motion were identified with separate localiser scans, using the procedure based on that described in Pitzalis et al. (2010); in which a coherent optic-flow stimulus (similar to the stimulus presented in the gradient condition in the main experiment, but the direction of motion changed randomly every 500 ms) and a random-motion stimulus were presented in 16-s blocks.

The ROIs were defined as all contiguous voxels that were significantly more active with a pattern of expansion-contraction and rotation (a coherent optic-flow stimulus), than with a random-motion stimulus; in the middle temporal cortex (MT+), the parieto-occipital sulcus (V6), the ventral intra-parietal area (VIP), the cingulate sulcus (CSv), the junction of the intraparietal sulcus (p2v), the region of the precuneus dorsal to the ascending arm of the cingulate sulcus motion area (PcM), and the posterior insular complex (PIC+).

2.5. Data analysis

All data were preprocessed and analysed with BrainVoyager QX (version 2.6, Brain Innovation, Maastricht, the Netherlands). EPIs were corrected for head motion and slice timing, and were filtered using a temporal high-pass filter with the cut-off of 3 cycles/run. No smoothing was applied. All functional images were aligned to the EPI acquired between the functional and anatomical scans. EPIs were first coregistered to the in-session MP-RAGE acquired with the 32-channel posterior-head coil. All images were then aligned to the reference MP-RAGE acquired with the full-head 32-channel phased-array coil, which were in alignment with the

anterior to posterior commissure (AC-PC) axis. To obtain the coordinates of ROIs in a normalised anatomical space, all data were subsequently transformed to Talairach space. Duration of vection/no-vection events and the timing of these events were derived from subjects' button presses.

Analysis was conducted by fitting a general linear model (GLM). Head-motion parameters were not included as GLM regressors. Every stimulus block and every vection/no-vection event were convolved with a canonical haemodynamic response function. It was then entered into a multiple-regression analysis to generate parameter estimates for each regressor at each voxel. Effect size (i.e. percentage blood-oxygen-level-dependent [BOLD] signal change) for the two conditions and the two sets of events were extracted for each independently defined ROI by averaging across all voxels in the ROI.

3. Results

3.1. Perceived vection

All subjects reported vection during optic-flow stimulation in the MRI scanner. The duration for which vection was perceived by each subject was averaged across four blocks of each experimental condition (i.e. gradient/no-gradient) and across 10 experimental runs (Figure 2). Vection was induced by both types of optic-flow stimulus with and without a speed gradient; however, two out of three subjects reported more sustained perception of vection in the gradient condition (HA: t (9) = 21.59, $p < 0.01$; JS: t (9) = 8.97, $p < 0.01$; BB: t (9) = 2.07, $p = 0.07$; two-tailed).

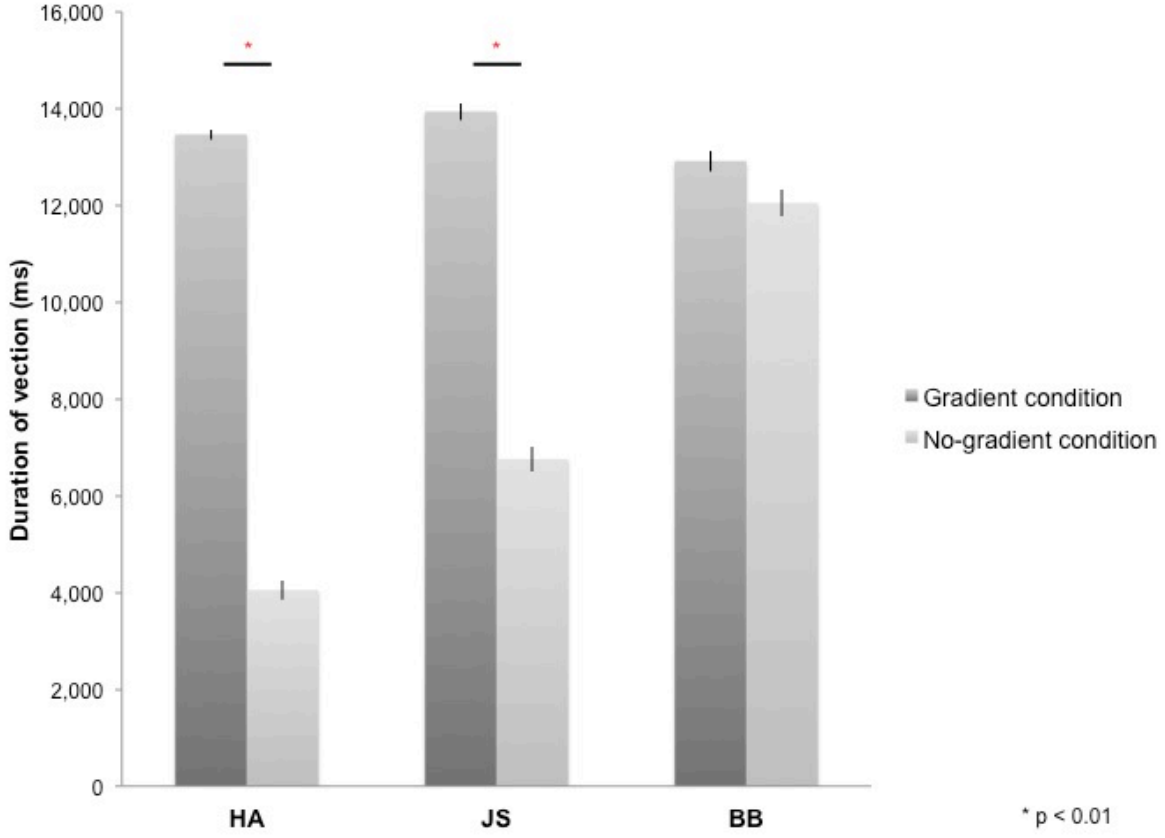

Figure 2. Duration of vection perceived during 16-s stimulus blocks in gradient and no-gradient conditions averaged over 10 runs for each subject. Error bars indicate standard error.

3.2. Functional localisation

To localise ROIs, BOLD responses to the coherent optic-flow and the random-motion stimuli were contrasted, which allowed for isolation of cortical sensory regions that are significantly more sensitive to coherent optic flow at *p*-value (uncorrected) of less than 0.005. The analysis was performed on the 3D anatomical volumes for each subject.

All seven ROIs were successfully identified bilaterally for all three subjects (Figure 3). The locations of those regions coincide with the Talairach coordinates of the counterparts reported in Cardin and Smith (2010). Mean Talairach coordinates for these ROIs are reported in Table 1, along with cluster sizes.

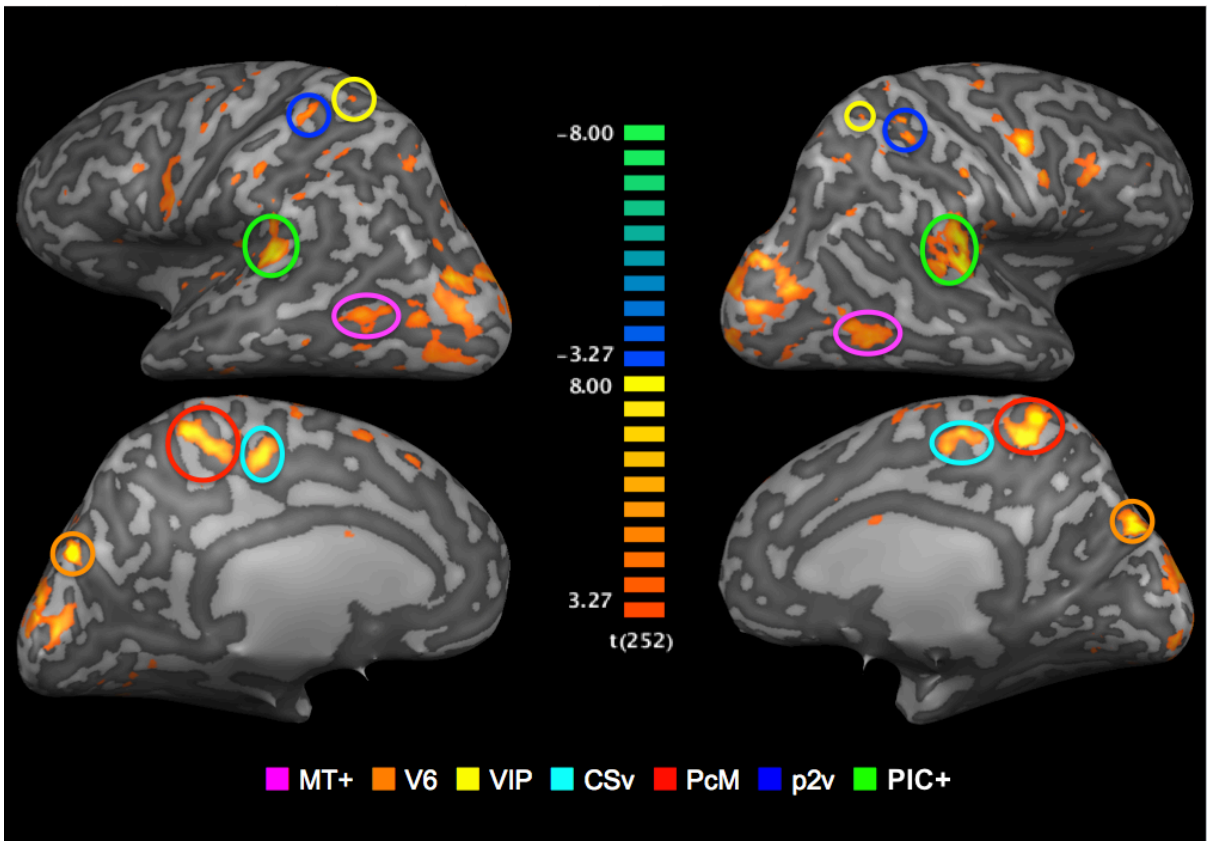

Figure 3. ROIs: Optic-flow selective sensory regions. The map of areas that showed a significantly greater response to optic-flow stimulus than to random-motion stimulus is superimposed onto inflated representations of the left and right hemispheres of one representative brain. T values are colour-coded (see colour bar). All activation shown is thresholded at $p < 0.005$ uncorrected.

Table 1. Mean Talairach coordinates and cluster sizes in voxels of ROIs.

Left	x	y	z	Cluster size	Right	x	y	z	Cluster size
MT+	-44	-62	1	368	**MT+**	45	-59	3	499
V6	-14	-81	22	284	**V6**	14	-80	27	467
VIP	-23	-56	44	74	**VIP**	20	-58	45	37
CSv	-14	-27	42	150	**CSv**	9	-27	46	119
PcM	-14	-49	47	74	**PcM**	8	-47	47	139
p2v	-30	-43	53	44	**p2v**	28	-42	53	47
PIC+	-50	-38	18	566	**PIC+**	49	-35	18	718

3.3. Main experiment

3.3.1. Effect of speed gradient

Speed gradients are one of the physical components of optic flow perceived during self-motion. To examine whether activity in the optic-flow selective areas is modulated by this physical property, activation in each ROI was contrasted between the gradient and the no-gradient conditions.

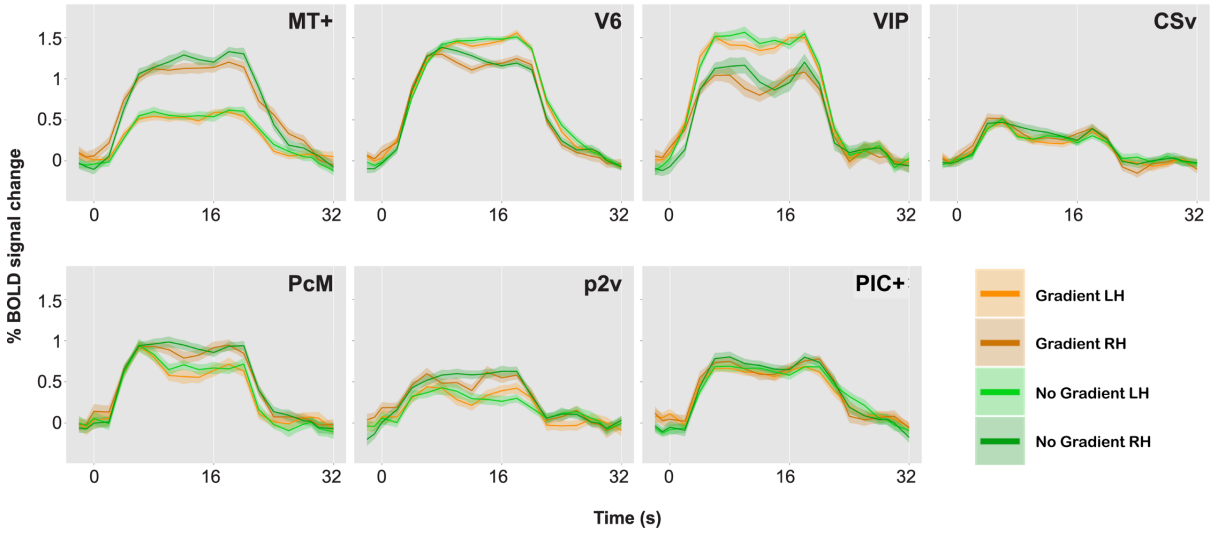

Figure 4. BOLD responses to optic-flow stimuli with and without speed gradient, for MT+, V6, VIP, CSv, PcM, p2v and PIC+ in one representative brain. Time series data for the two conditions and for the two hemispheres are overlaid. A single time series was computed from 10 runs. The time series was then collapsed over a single stimulus cycle of 32 s: The stimulus-presentation block lasted from 0 to 16 s followed by a 16-s ISI. Error bars indicate standard error.

Figure 4 represents the percent signal changes in the gradient and the no-gradient conditions in one of the subjects. All seven ROIs in all hemispheres showed positive BOLD responses to optic-flow stimulation in both the gradient and the no-gradient conditions, which confirms the sensitivity and selectivity of those areas to optic flow documented in the literature (Cardin & Smith, 2010; 2011). In order to examine whether any of ROIs showed differential responses to optic-flow stimuli with and without speed gradient, an event-related average time series was computed for each of the 10 experimental runs for each ROI, and magnitude of BOLD responses between 5 s after the stimulus onset and 4 s after the stimulus offset was averaged for both conditions. Consequently, there were 10 data points per condition per ROI. A paired two-sample t-test (two-tailed) was performed for each ROI in each subject. The results of the t-tests are reported in Table 2.

As can be seen in Table 2, few of the ROIs exhibited differential activation between the gradient and the no-gradient conditions. The neural responses were similar in the two conditions in most/all of ROIs in all three subjects (Table 2); the exceptions were areas CSv ($t(9) = 2.78$, $p = 0.02$) and PcM ($t(9) = 3.49$, $p = 0.007$) in the right hemisphere of one subject, and area MT+ ($t(9) = 2.39$, $p = 0.04$) in the right hemisphere of another. There was no consistency in areas that showed a significant difference between the two conditions across subjects.

Table 2. Results of comparison of BOLD responses between gradient and no-gradient conditions.

Test statistics (*t*) and *p*-level (in parentheses) are reported for each ROI.

Subject	Hemisphere	MT+	V6	VIP	CSv	PcM	P2v	PIC+
HA	**LH**	0.30 (0.77)	1.17 (0.27)	1.27 (0.24)	0.72 (0.49)	1.27 (0.24)	1.80 (0.11)	1.79 (0.11)
	RH	1.43 (0.19)	0.72 (0.49)	0.50 (0.70)	2.78 (0.02) *	3.49 (0.007) **	1.71 (0.12)	1.87 (0.09)
JS	**LH**	-1.54 (0.16)	-0.02 (0.98)	-0.40 (0.70)	-0.61 (0.56)	0.32 (0.76)	-1.95 (0.08)	0.17 (0.87)
	RH	-2.11 (0.06)	-0.13 (0.90)	0.01 (0.99)	-0.23 (0.82)	0.87 (0.41)	-1.13 (0.29)	-1.48 (0.17)
BB	**LH**	0.66 (0.53)	0.49 (0.63)	1.26 (0.24)	0.50 (0.63)	0.94 (0.37)	0.34 (0.74)	0.62 (0.54)
	RH	2.39 (0.04) *	0.76 (0.47)	1.20 (0.26)	0.17 (0.87)	1.05 (0.32)	1.97 (0.08)	0.83 (0.43)

* $p < 0.05$, ** $p < 0.01$

3.3.2. Effect of vection

In order to assess the role of optic-flow selective areas in visuo-vestibular integration, and therefore in the processing of optic flow as a cue to self-motion, activation during the vection events was measured against that during the no-vection events.

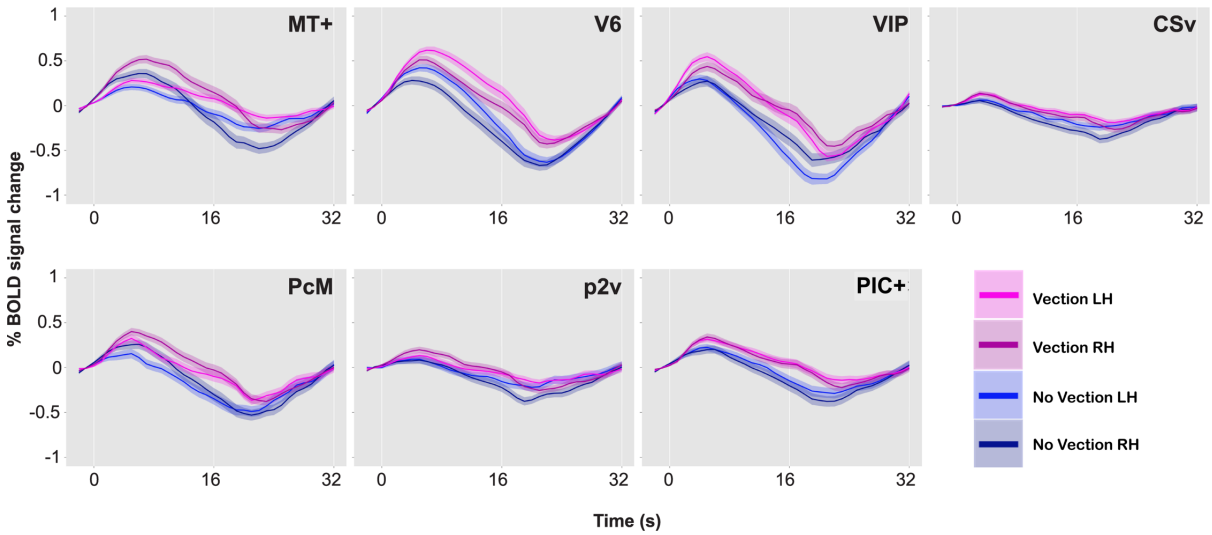

Figure 5. BOLD responses during vection and no-vection events, for MT+, V6, VIP, CSv, PcM, p2v and PIC+ in one representative brain. Time series data for the two types of events and for the two hemispheres are overlaid. A single time series was computed from 10 runs. The time series was then collapsed over a single cycle of 32 s. Error bars indicate standard error.

Figure 5 illustrates the percent signal changes during the vection and the no-vection events in one of the subjects. A paired two-sample t-test (two-tailed) was performed for each ROI in each subject to compare activity in each area during the vection events to that during the no-vection events. For both sets of events, an event-related average time series was computed for each of the 10 experimental runs for each ROI, and magnitude of BOLD responses across 10 s

from 5 s after the button press was averaged. Consequently, there were 10 data points per type of events per ROI. The results of the t-tests are reported in Table 3.

A comparison of BOLD responses between the vection and the no-vection events in each ROI yielded that magnitude of activation in areas including MT+, V6, VIP and PIVC was significantly larger during periods of self-reported perception of vection (Table 3). Those four areas exhibited differential activation in more than four of the six hemispheres.

Table 3. Results of comparison of BOLD responses during self-reported states of vection and no-vection. Test statistics (*t*) and *p*-level (in parentheses) are reported for each ROI.

Subject	Hemisphere	MT+	V6	VIP	CSv	PcM	P2v	PIC+
HA	**LH**	2.88 (0.02) *	2.53 (0.03) *	1.98 (0.08)	2.30 (0.04) *	1.98 (0.07)	0.27 (0.79)	3.15 (0.01) *
	RH	3.77 (0.004) **	3.29 (0.009) **	3.53 (0.006) **	1.03 (0.33)	1.87 (0.09)	-0.58 (0.58)	2.37 (0.04) *
JS	**LH**	1.69 (0.13)	2.33 (0.04) *	1.97 (0.08)	1.48 (0.17)	1.77 (0.11)	0.59 (0.57)	-0.09 (0.93)
	RH	2.19 (0.06)	2.25 (0.05)	2.40 (0.04) *	1.68 (0.13)	2.06 (0.07)	1.11 (0.29)	2.89 (0.02) *
BB	**LH**	2.36 (0.04) *	4.02 (0.003) **	4.79 (0.001) **	3.27 (0.01) **	4.36 (0.002) **	2.61 (0.03) *	3.61 (0.006) **
	RH	3.55 (0.006) **	3.98 (0.003) **	3.20 (0.01) *	4.40 (0.002) **	3.85 (0.004) **	4.33 (0.002) **	4.93 (0.001) **

* $p < 0.05$, ** $p < 0.01$

4. Discussion

4.1. Functional localisation of ROIs

Results confirm the effectiveness of the functional localiser employed in this study, which is based upon that proposed by Pitzalis et al. (2010), in localising not only V6 but also other optic-flow selective regions (Cardin & Smith 2010, 2011). It is interesting to note that, contrarily to what has been suggested in the literature (Pitzalis et al. 2006; Cardin et al. 2012), the results suggest that wide-field stimulation is not necessarily crucial for localisation of V6 as well as other optic-selective areas.

4.2. Speed gradient vs. perceived vection

The comparison of activity in ROIs between the gradient and the no-gradient conditions yielded unremarkable results: There was not one area that consistently responded differently to optic-flow stimuli with and without a speed gradient across subjects. Speed gradients are one of the defining factors of optic flow that makes it consistent with optic-flow stimulation that is experienced by an observer during actual self-motion, and this indeed modulated the duration of vection perceived by subjects during the experiments. The lack of clear difference in BOLD responses between the gradient and the no-gradient conditions, however, suggests that these cortical sensory areas are not simply modulated by this physical property of optic flow.

The principal purpose of these experiments was to assess whether optic flow is encoded differently according to the presence or absence of vection. Results of the contrast between

BOLD responses during the vection and the no-vection events show that there are several optic-flow selective regions that respond more robustly during self-reported perceptual states of vection. These areas include visual areas MT+ and V6, and the polysensory areas VIP and PIC+.

4.3. Visual areas MT+ and V6

Because both MT+ and V6 have been shown to possess selectivity towards coherent optic-flow stimuli (Dukelow et al. 2001; Huk et al. 2002; Morrone et al. 2000; Wall & Smith 2008; Pitzalis et al. 2010; Cardin & Smith 2010, 2011), they might be expected to show consistent activation regardless of whether vection is experienced. However, in line with previous findings (Kovacs et al. 2008; Wall & Smith 2008; Cardin & Smith 2010), differential activation was observed in visual areas MT+ and V6 depending on the presence or absence of vection.

The most plausible explanation for these results may be that those visual areas receive feedback from the polysensory areas (e.g. VIP) that receive direct input from vestibular areas such as PIVC (Lewis and van Essen 2000). Although evidence in the human brain is limited, there are findings in the monkey brain that indicate that MT+ is anatomically and functionally connected to the polysensory areas VIP (Mansell & van Essen, 1983; Undergleider & Desimone, 1986; Boussaoud et al., 1990; Braizer et al., 1991) and the precuneus (Blum et al. 1950; Leichnetz, 2001). Furthermore, MT+ and V6 in the human brain have recently been found to be anatomically connected via ventral occipital fasciculus (VOF: Yeatman et al. 2014; Takemura et al. 2016). This reciprocal relationship between the visual and polysensory areas would allow for integration of optic flow and vestibular cues to self-motion to be processed more efficiently.

4.4. Polysensory areas VIP and PIC+

4.4.1. VIP

Results also indicate that the polysensory area VIP respond differently to optic flow during the periods in which vection is perceived. This area is considered a part of the dorsal visual pathway in the monkey brain (Felleman & van Essen 1991); and has been shown to consist of a substantial number of polysensory neurons, and to respond to visual, vestibular as well as somatosensory stimulation (Duhamel et al. 1998; Bremmer et al. 2001a, 2001b). It has also been suggested that VIP receive visual projection from MT+ (Maunsell & van Essen 1983; Underleider & Desimone 1986) and vestibular projection from PIVC (Lewis & van Essen 2000) in the monkey brain.

4.4.2. PIC+

The polysensory area PIC+ (Guldin & Grusser 1998) also showed differential activation during states of vection, which suggests that PIC+ encodes optic flow differently depending on the presence or absence of vection. This agrees with previous findings (Brandt et al. 1999; Kleinschmidt et al. 2002; Deutschlander et al. 2004; Indovina et al. 2005; Kovacs et al. 2008) that the activity in PIC+ reflects the sensation of self-motion.

It should be noted, however, in contrast to the findings of a number of previous studies (Brandt et al. 1998; Kleinschmidt et al. 2002; Deutschlander et al. 2004), increased rather than decreased activity was observed in PIC+. This discrepancy in the findings could be due to the motion components that constituted the optic-flow stimuli used in this study. Unlike in some

of the previous studies, which used constant-velocity stimuli with single motion component, the stimuli used in this study consisted both changing linear-motion (i.e. expansion and contraction) and rotational-motion components in order to maximise BOLD responses in the ROIs. It has been shown that PIC+ responds selectively to body acceleration (Nishiike et al. 2002; Indovina et al. 2005); therefore, it is likely that using stimuli with a dynamic pattern of motion compatible with continuously changing body acceleration (in forward, backward and rotating directions) lead to robust and positive BOLD responses in PIC+ as well as stronger visuo-vestibular interaction observed in this study. Otherwise, this inconsistency may have arisen from the controversy over the definitions of PIC+ and PIVC. As outlined in Greenlee et al. (2016), the definitions of PIC+ and PIVC in the human brain seem to have been confounded. They suggest that the previously reported suppression in the posterior lateral sulcus by visual motion cues can be explained by the fact that PIVC is a purely vestibular area, whereas previously reported activation during self-motion induced by visual motion cues in the posterior lateral sulcus might fall within PIC, which is predominantly visual but also receives vestibular inputs (Frank et al., 2014; Frank et al. 2016; Greenlee et al. 2016).

Taken together, these findings and the results of this study place the polysensory areas VIP and PIC+ in a good position to integrate visual cues related to self-motion and vestibular information (or lack thereof). The possibility that those polysensory areas integrate sensory information and is an extremely important area for processing self-motion is further supported by the findings that VIP interacts with premotor area (Klam & Graf 2003; Schlack et al. 2002) of which function is to execute motion that is driven by sensory information.

4.5. Individual differences

Kennedy et al. (1996) demonstrated that there are vast individual differences in the magnitude of vection experienced and the duration for which perception of vection lasts.

One subject who was extremely susceptible to vection coincidentally exhibited the largest and most persistent differential activation in the areas discussed above according to the presence or absence of vection. It is possible that the individual differences in brain activity reflect those observed at the behavioural level; however, it is difficult to draw any inference from the results of this study alone. In order to address this question, not only the duration of perceived vection but also the magnitude of vection should be taken into account and it is critical that those measures are directly correlated with brain activity.

4.6. Future directions

The findings not only dissociate the roles of and interaction between the cortical sensory regions of interest related to optic-flow stimulation from those related to sensation of self-motion, but also contribute to discussion on multisensory integration processes underlying perception of vection. Future studies should aim to validate and strengthen evidence for this multisensory mechanism, possibly by introducing analyses such as multi-voxel pattern analysis (MVPA). Inclusion of MVPA could shed new light to the interpretation of the data by increasing sensitivity to changes in cortical activation between the two perceptual states of vection and no vection (Arnoldussen et al. 2013).

5. Conclusion

The present study investigated how vection is represented in the optic-flow selective sensory areas, in order to determine which of those areas are involved in the integration of optic flow and vestibular cues to self-motion. It was found that visual areas MT+ and V6, polysensory areas VIP and PIC+ seems to encode optic flow differently when optic-flow processing is accompanied by a sensation of self-motion, which suggests that VIP and PIC+ are the most likely candidates for areas that integrate optic flow and vestibular information related to self-motion.

Chapter 3: Stratum proprium of interparietal sulcus supports communication between optic-flow selective areas involved in visuo-vestibular integration

1. Introduction

Optic-flow processing is one of the cortical functions that involve the parietal cortex. A network of sensory areas in the parietal cortex has been shown to be involved in optic-flow processing (Cardin & Smith 2010, 2011). Those optic-flow selective areas include the ventral intraparietal area (VIP), the precuneus motion area (PcM) and the putative area 2v (p2v) located in the superior part of the parietal cortex, and the posterior-insular complex (PIC+: Deutschländer et al. 2004; Cardin & Smith 2010, 2011; Biagi et al. 2015; Wada et al. 2016) in the inferior part of the parietal cortex. Several studies have described a convergence of visual and vestibular information regarding self-motion, involving those optic-flow selective areas (Kleinschmidt et al. 2002; Wiest et al. 2004; Kovács et al. 2008; Fetsch et al. 2009; Butler et al. 2010; Prsa et al. 2015; Uesaki & Ashida 2015; Wada et al. 2016). In order to fully understand the underlying mechanism of optic-flow processing, it is essential to investigate

how communication between the superior and inferior parts of the parietal cortex is supported by the white matter anatomy.

Here, we focus on a short white matter tract connecting the superior and inferior parts of the parietal cortex, wrapping around the inferior parietal sulcus. This tract was initially described by the German neurologist Heinrich Sachs (1892) as *the stratum proprium of interparietal sulcus* (hereafter, we refer to this tract as SIPS). Except for one recent fibre dissection study replicating Sachs's work (Vergani et al., 2014), this tract has been largely overlooked in the literature. Given the functional MRI (fMRI) evidence indicating the involvement of the superior and inferior parts of the parietal cortex in crucial cognitive functions (Corbetta & Shulman 2002; Culham et al., 2006; Uncapher & Wagner 2009; Cardin & Smith 2010; Blanke 2012; Greenlee et al. 2016), SIPS is a necessary and important tract supporting those functions. In particular, Chapter 2 suggests that VIP in the superior part of the parietal cortex and PIC+ in the inferior part of the parietal cortex may be the loci of visuo-vestibular integration underlying optic-flow processing and perception of self-motion. Yet, the characteristics of SIPS are poorly understood due to the lack of studies replicating SIPS in the living human brain, using three-dimensional digital anatomical data such as dMRI and reproducible computational analyses.

We used dMRI and tractography to identify the anatomical location and trajectory of SIPS in the living human brain. The ensemble tractography (Takemura, Caiafa, et al. 2016) yielded bilateral identification of SIPS in all 10 subjects. Evidence for SIPS was evaluated based on the consistency across datasets, comparison with post-mortem fibre dissection studies (Sachs 1892; Vergani et al. 2014), and the virtual lesion analysis (Pestilli et al. 2014; Leong et al. 2016; Gomez et al. 2015; Takemura, Rokem et al. 2016). We also explored the functional

relevance of SIPS by performing fMRI experiments on the same subjects and examining the spatial proximity between the SIPS endpoints and functionally-defined cortical areas previously associated with optic-flow processing (Cardin & Smith, 2010, 2011; Greenlee et al. 2016). Results showed that the dorso-lateral SIPS endpoints are near VIP, PcM and p2v, whereas the ventro-medial SIPS endpoints are near PIC+; placing SIPS in a good position to channel sensory signals between the distant cortical areas underlying visuo-vestibular integration necessary for optic-flow processing and perception of self-motion. Finally, we also demonstrate evidence of SIPS in additional 90 subjects from publically available HCP datasets.

2. Materials and methods

We analysed dMRI data of 100 human subjects, from three independent datasets. One set of dMRI data was acquired at Kokoro Research Center, Kyoto University (KU dataset), along with fMRI measurements to identify cortical regions activated by optic-flow stimulation. The other dMRI datasets were obtained from the Human Connectome Project (HCP) by WU-Minn Consortium (WU-Minn HCP; Van Essen et al. 2013) and MGH-USC Consortium (MGH-USC HCP; Fan et al. 2016).

2.1. Subjects: KU Dataset

Six healthy volunteers (three males and three females; of the ages between 22 and 47 years; subjects S1-S6) participated in the study. All six subjects underwent both dMRI and fMRI experiments. All had normal or corrected-to-normal vision. All individual subjects gave written informed consent to take part in this study, which was conducted in accordance with the ethical

standards stated in the Declaration of Helsinki and approved by the local ethics and safety committees at Kyoto University.

2.2. Data acquisition and preprocessing: KU Dataset

All MR images were obtained with a 3-Tesla Siemens Magnetom Verio scanner (Siemens, Erlangen, Germany), using a Siemens 32-channel head coil, at Kokoro Research Center, Kyoto University.

2.2.1. Diffusion-weighted MRI data

Two repeated acquisitions of MR images were conducted for each subject, using a diffusion-weighted single-shot spin echo, echo-planar sequence (60 axial slices, 2-mm isotropic voxels, time of repetition (TR) = 8300 ms, time echo (TE) = 94 ms, field of view (FoV) = 200 x 200 mm^2). The dMRI data were sampled in 64 directions with a b-value of 1000 s/mm^2. Two non-diffusion weighted images (b = 0) were obtained.

Diffusion data were preprocessed using mrDiffusion, implemented in Matlab as part of the mrVista software distribution (https://github.com/vistalab/vistasoft). MR images in each scan were motion-corrected to the b = 0 image acquired in the same scan, using a rigid-body alignment algorithm implemented in SPM (Friston & Ashburner 2004). Eddy-current correction and head-motion correction were applied in the process of 14-parameter constrained nonlinear coregistration, based on the expected patterns of eddy-current distortion given the phase-encoding directions of the acquired data (Rohde et al. 2004). The gradient direction in each diffusion-weighted volume was corrected using the rotation parameters from the motion

correction procedure. Subsequently, fibre orientation in each voxel was estimated using constrained spherical deconvolution (CSD; Tournier et al. 2007; L_{max} = 8) implemented in MRtrix (Tournier et al. 2012). CSD allows for tractography based on a model that is capable of accounting for crossing fibres. Because the tract connecting the superior and inferior parts of the parietal cortex likely intersects with the neighbouring major fasciculi such as the arcuate fasciculus, CSD was employed to fully reconstruct the tract.

2.2.2. T1-weighted image data

For each subject, a high-resolution T1-weighted 3D anatomical image was acquired with a magnetisation-prepared rapid-acquisition gradient echo (MP-RAGE; 208 axial slices, 1-mm isotropic voxels, TR = 2250 ms, TE = 3.51 ms, FoV = 256 x 256 mm^2, flip angle = 9°, bandwidth = 230 Hz/pixel), and the border between the grey matter and white matter was defined. Initial segmentation was performed using an automated procedure in Freesurfer (Fischl 2012), which was then refined manually (Yushkevich et al. 2006).

2.2.3. Functional data and localisation of optic-flow selective sensory regions

In order to determine the spatial relations between the white matter tract and the optic-flow selective sensory areas (Cardin & Smith 2011; Frank et al. 2014), four regions of interest (ROIs) were identified with data acquired in separate fMRI localiser scans, using the procedure described in Chapter 2. The stimulus was a random dot kinematogram consisting of 200 moving light dots of 10 x 10 pixels (subtending approximately 0.4° x 0.4° visual angle) on a dark background. The dots initially appeared at random locations and formed a circular patch of 30° diameter. Motion directions of the dots were arranged so that the dots (a) cycled through

a spiral space with time-varying trajectories away from and towards the centre of the patch for the optic-flow stimulus, or (b) moved in random directions for the random-motion stimulus. The coherent optic-flow and random-motion stimuli were presented in 16-s blocks. Subjects maintained central fixation throughout the experiment. No attentional task was undertaken.

Functional data were acquired with a gradient echo, echo-planar sequence (39 contiguous axial slices, 3-mm isotropic voxels, TR = 2000 ms, TE = 25 ms, FoV = 192 x 192 mm^2, flip angle = 80°, bandwidth = 2368 Hz/pixel), using a Siemens 32-channel posterior-head array coil; which gave an improved signal-to-noise ratio in the occipital cortex at the expense of the anterior part of the brain. Each subject underwent two fMRI scans. Functional data were then preprocessed and analysed with BrainVoyager QX (version 2.6, Brain Innovation, Maastricht, the Netherlands). Analysis was conducted by fitting a general linear model (GLM). Each of the 16-s stimulus blocks was convolved with a canonical haemodynamic response function, and entered into a multiple-regression analysis to generate parameter estimates for each regressor at each voxel. Blood-oxygen level dependent responses to the coherent optic-flow and random-motion stimuli were contrasted, which allowed for isolation of cortical regions that are significantly more sensitive to coherent optic flow at p-value (uncorrected) of less than 0.005. The analysis was performed on the 3D anatomical volumes for each subject. The ROIs were defined as all contiguous voxels that were significantly more active with coherent optic-flow stimulation than with random-motion stimulation (Uesaki & Ashida 2015); in the ventral intra-parietal cortex (VIP), the precuneus motion area (PcM), the junction of the intra-parietal sulcus (p2v), and the posterior region of the insular cortex (PIC+). Stimulus design and analysis methods are described in more detail elsewhere (Uesaki & Ashida 2015).

2.3. Data acquisition and preprocessing: Human Connectome Project datasets

Diffusion-weighted MRI data obtained from 61 subjects in WU-Minn HCP dataset (S7-S67: Van Essen et al. 2013) and 33 subjects in MGH-USC HCP dataset (S68-S100: Fan et al. 2016) were also analysed in this study. These data were acquired with multiple b-values (1000, 2000 and 3000 s/mm^2 for WU-Minn HCP dataset; 1000, 3000, 5000 and 10000 s/mm^2 for MGH-USC HCP dataset), high spatial (1.25 x 1.25 x 1.25 mm^3 for WU-Minn HCP dataset; 1.5 x 1.5 x 1.5 mm^3 for MGH-USC HCP dataset) and angular resolution (90 directions at each b-value for WU-Minn HCP dataset; 64 directions at b = 1000, 3000 s/mm^2 and 128 directions at b = 5000, 10000 s/mm^2 for MGH-USC HCP dataset). We note that the selected HCP data were acquired with greater spatial and angular resolution, and higher b-values compared with KU dataset. All HCP data were preprocessed by WU-Minn HCP and MGH-USC HCP Consortiums using methods that are described in Sotiropoulos et al. (2013) and Fan et al. (2014), respectively.

2.4. Data analysis

2.4.1. Coregistration of functional and diffusion MR images to T1-weighted images

T1-weighted 3D anatomical images were aligned to the anterior commissure-posterior commissure (AC-PC) plane. To do this, the locations of AC and PC were manually defined in the T1-weighted images. These landmarks were then used to apply rigid-body transformation to align the anatomical images to the AC-PC plane.

Preprocessed fMRI and dMRI data were coregistered to the T1-weighted images in the AC-PC space, using a two-stage coarse-to-fine approach. This process enabled a direct spatial comparison between the tract endpoints and the ROIs within the same coordinates in each subject, in the later analyses.

2.4.2. Tractography

We used two complementary approaches to perform tractography. One is the ensemble tractography (Takemura, Caiafa et al. 2016) based on the linear fascicle evaluation (LiFE; Pestilli et al. 2014; http://francopestilli.github.io/life/), which generates streamlines with various tractography parameters and removes those that do not contribute to predicting the diffusion signals. The advantage of this approach is that spurious streamlines that do not explain diffusion signals are not included in the resulting model. It also allows for evaluation of statistical significance of the estimated tract based on cross-validation (virtual lesion analysis; Pestilli et al. 2014; Takemura, Rokem et al. 2016; Leong et al. 2016). However, this approach requires a large amount of computational resources to optimise large-scale linear matrices composed of diffusion signals in every voxel acquired with multiple angular directions, as well as a mass of candidate streamlines (Takemura, Caiafa et al. 2016). This makes it less practical to apply this framework to analysing data from large samples, until the ongoing work to reduce the necessary computational load of LiFE is completed (Caiafa & Pestilli 2017). Another limitation is that the current implementation of LiFE only accepts single-shell dMRI data (Pestilli et al., 2014).

The alternative approach is to exclude the ensemble tractography and LiFE from the analysis pipeline. At a cost of opting out statistical evaluation using the identical methods, we analysed

the data of a large sample (i.e. 100 subjects) to assess the generality of our findings. Additionally, this alternative approach has a distinct advantage over the ensemble tractography and LiFE analyses, which is that it allows for tracking algorithms based on multi-shell dMRI data (Jeurissen et al., 2014). These two approaches can be complementary in validating the findings; one is designed to evaluate the statistical evidence on smaller samples, whereas the other simpler pipeline is well-suited for assessing the generality across a larger number of subjects.

2.4.2.1. Ensemble tractography

For the six subjects of KU dataset (S1-S6) and four subjects from WU-Minn HCP dataset (S7-S10), we used the ensemble tractography (Takemura, Caiafa, et al. 2016) to estimate the white matter tract based on dMRI data from each subject. Measurements from the 2000 s/mm^2 shell were extracted from the original WU-Minn HCP dataset and used for analyses.

Candidate streamlines were generated with MRtrix (Tournier et al. 2012), using CSD-based probabilistic tractography (step size = 0.2 mm; maximum length = 200 mm; minimum length = 10 mm; fibre orientation distribution (FOD) amplitude stopping criterion = 0.1). We used the entire grey matter-white matter interface region as a seed (Smith et al. 2012), and the seed voxels were randomly selected from the mask for generating candidate streamlines. Tracking was terminated when a streamline reached outside the white matter mask. We used four different anglular threshold settings (angular threshold = 5.7, 11.5, 23.1, 47.2 deg). Two million candidate streamlines were generated for each curvature parameter setting. We then selected those located within the white matter posterior to the most anterior optic-flow selective area

(the cingulate sulcus visual area; CSv; Cardin & Smith 2010; Smith et al. 2017) in each hemisphere, which were used in all subsequent analyses.

In order to obtain an optimised connectome model comprising streamlines generated with different curvature thresholds, we used the preselection method of the ensemble tractography (Takemura, Caiafa, et al. 2016). First, we separately optimised each connectome generated with a single curvature parameter using LiFE. We then selected 150,000 streamlines that contributed meaningfully to predicting the diffusion signals from each single-parameter connectome, and combined them to create a new candidate connectome (the ensemble tractography connectome; ETC; 600,000 candidate streamlines) in each hemisphere. Finally, LiFE was applied again to optimise the ETC. As a result, the optimised ETC included 103,664 streamlines on average per hemisphere. The optimised ETC has been shown to perform better than conventional connectome models, in terms of model accuracy and anatomical representation (Takemura, Caiafa, et al. 2016; https://github.com/brain-life/ensemble_tractography). Optimised ETCs were used for identification and validation of SIPS.

2.4.2.2. Tractography analysis of a large sample

For dMRI data of the other 90 subjects (56 subjects from WU-Minn HCP and 34 subjects from MGH-USC HCP datasets), we performed probabilistic tractography based on multi-tissue CSD implemented in MRtrix (Jeurissen et al., 2014; step size: 0.625 mm for WU-Minn HCP, 0.75 mm for MGH-USC HCP; angular threshold: 45 deg; minimum length: 2.5 mm for WU-Minn HCP, 3 mm for MGH-USC HCP; maximum length: 250 mm; FOD amplitude stopping criterion = 0.1). Measurements of all b-values are used for estimating multi-tissue CSD. We

used the entire grey matter-white matter interface region as a seed (Smith et al. 2012), and the seed voxels were randomly selected from the mask for generating candidate streamlines. Tracking was terminated when a streamline reached the white matter mask. As a result, two million streamlines were generated. LiFE was not applied in this analysis.

2.4.3. Tract segmentation

We used the cortical ROIs defined by Freesurfer segmentation (Desikan-Killiany atlas; Desikan et al. 2006) to identify the white matter tract connecting the superior and inferior parts of the parietal cortex in the optimised connectome. For the main analysis, two cortical ROIs, one in the superior parietal cortex and the other in the inferior parietal cortex were created. The ROI in the superior part of the parietal cortex was defined as a combination of two Freesurfer ROIs, "precuneus" and "superior_parietal", because these two ROIs combined covered the positions of the functionally identified areas located in the superior parietal cortex (VIP, PcM, p2v). The Freesurfer ROI labelled "supramarginal gyrus" was used as the ROI in the inferior parietal cortex, which covered the general region including PIC+.

The tract between the superior and inferior parts of the parietal cortex was identified as a group of streamlines having one of the endpoints near the superior parietal ROI and the other near the inferior parietal ROI (within 3 mm from each grey matter ROI; i.e. within two voxels from each grey matter ROI in KU, MGH-USC HCP datasets and three voxels in WU-Minn HCP dataset). Only streamlines terminating near the grey matter ROIs and not those passing through the grey matter ROIs were included, since tractography was anatomically constrained by the grey matter-white matter interface region used as a seed in generating candidate streamlines and did not allow for streamlines passing through the grey matter-white matter boundary to be

generated (Smith et al. 2012). The segmented tract was then refined by removing outlier streamlines. Those were streamlines that met the following criteria: (1) streamlines longer than the mean streamline length of the tract by ≥ 3 sd; (2) streamlines shorter than 15 mm; (3) streamlines, of which positions are ≥ 3 sd away from the mean position of the tract (Yeatman, Dougherty, Myall, et al. 2012).

The MATLAB code used to identify SIPS in this study is available in Github repository (https://github.com/htakemur/SIPS) and also as part of AFQ toolbox (Yeatman, Dougherty, Myall, et al. 2012; https://github.com/yeatmanlab/AFQ).

2.4.4. Estimating cortical endpoints of the tract

Streamlines terminate at the boundary between the white matter and grey matter. In order to estimate the SIPS endpoints in the cortical surface representation, the coordinates of the SIPS endpoints were collected, and the distance between those coordinates and the grey matter voxels was calculated. For each grey matter voxel, the number of the SIPS endpoints falling within a threshold distance (3 mm) was counted. The normalised endpoint counts are plotted on the inflated cortical surface in Figure 6B. The same method was used in Takemura, Rokem et al. (2016).

2.4.5. Virtual lesion analysis

We conducted the virtual lesion analysis (Pestilli et al. 2014; Leong et al. 2016; Takemura, Rokem, et al. 2016) on KU dataset to evaluate the statistical evidence supporting the existence of the white matter tract connecting the superior and inferior parts of the parietal cortex. For

this analysis, we divided the dMRI data (KU dataset) into two sessions; one was used for performing tractography, and the other was used for computing cross-validated model prediction accuracy.

Two connectome models were used in the analysis; the optimised connectome and a lesioned connectome with the streamlines of interest (i.e. the streamlines that belong to the tract connecting the superior and inferior parts of the parietal cortex) removed. We computed prediction accuracy (root mean squared error; RMSE) of those models in predicting the diffusion signals. The set of dMRI data from the second session was used as the measured diffusion signals for cross-validation. Model accuracy is described as a ratio of RMSE (R_{rmse}), and it represent prediction accuracy of each model with respect to test-retest reliability (for calculation methods, see Rokem et al. 2015; Takemura, Caiafa, et al. 2016). $R_{rmse} = 1$ indicates that the model accuracy for predicting the diffusion signals in the second dataset equals to test-retest reliability of the diffusion signals in the same voxel.

R_{rmse} was compared in all voxels touched by the lesioned streamlines (the streamlines that belong to SIPS). The complete set of streamlines that contribute to the prediction of the diffusion measurements in those voxels is called the path-neighborhood of SIPS (Wedeen et al. 2012). This path-neighborhood includes SIPS itself and all of the other streamlines that pass through the voxels SIPS passes through. We calculated the distribution of R_{rmse} values in SIPS voxels with the entire path-neighborhood included and removed SIPS, to figure out the weight of each of the remaining streamlines.

Evidence supporting SIPS was assessed using two different measures. We compared the two R_{rmse} distributions using the strength of evidence, *S,* which is the difference in the mean R_{rmse} divided by the joint standard deviation (for technical detail, see Pestilli et al. 2014).

2.4.6. Spatial proximity between SIPS endpoints and functionally-defined ROIs

In order to characterise the spatial proximity between the optic-flow selective ROIs and SIPS, we measured the proportion of grey matter voxels in each ROI (VIP, PcM, p2v and PIC+) located adjacent to the SIPS endpoints. We computed the three-dimensional distance between the endpoints of each SIPS streamline and each grey matter voxel included in the ROIs. We then calculated the proportion of voxels in each ROI located within a specific distance (thresholded at 3 or 4.5 mm in volumetric space) from any SIPS endpoints. This procedure is based on that reported in Takemura, Rokem, et al. (2016).

We note that there are limitations to this analysis, due to the general difficulty in associating streamline endpoints and the grey matter surface (Reveley et al. 2015), particularly for dMRI data with a standard resolution such as those used in this study (i.e. KU dataset). The aim of this analysis was to examine the general spatial proximity between the tract endpoints and functionally defined ROIs, rather than to determine the projection pattern of the tract on the cortical surface.

2.4.7. Probabilistic atlas of SIPS

We created the probabilistic atlas of SIPS based on our 100-subject dataset following the method proposed in previous works (Bürgel et al. 2006; Catani & Thiebaut de Schotten 2012). The b = 0 images of each subject were normalised to the Montreal Neurological Institute 152 (MNI152) space using the MNI152 EPI template in order to obtain the affine transformation matrix. We then generated a binary visitation map of SIPS in each subject by assigning a value

of 1 or 0 to each voxel depending on whether the voxel is intersected by any SIPS streamlines (Catani et al. 2007; Thiebaut de Schotten 2008). This binary visitation map was normalised to MNI152 space according to the transformation matrix derived from the normalisation of the b = 0 images. Finally, we computed the percentage overlap by summing the normalised visitation maps of all subjects at each point in MNI152 space (Bürgel et al. 2006; Catani & Thiebaut de Schotten 2012). Figures 2.4 show the visualisation of the percentage overlap with the overlap threshold at greater than 25% of the sample.

3. Results

The primary aim of this study was to identify a white matter tract connecting the superior and inferior parts of the parietal cortex. By performing tractography on the dMRI data, we successfully identified SIPS in all subjects. We compared the tractography estimates with SIPS reported in the post-mortem fibre dissection studies (Sachs 1892; Vergani et al. 2014), and evaluated the statistical evidence for the estimates (Pestilli et al. 2014) as well as consistency across datasets. The tract was identified consistently across subjects and across datasets, and seems to correspond with the tract referred to as SIPS in previous fibre dissection studies (Sachs 1892; Vergani et al. 2014). Furthermore, we assessed the spatial relations between SIPS and the optic-flow selective sensory areas localised using fMRI.

3.1. Anatomy of human SIPS

3.1.3. Tract trajectory and length

We analysed dMRI data of the six subjects from KU dataset using the ensemble tractography (Takemura, Caiafa, et al. 2016; see Materials and methods), whereby streamlines were generated using multiple parameter settings, and then optimised using LiFE (Pestilli et al. 2014; see Materials and methods). We identified a white matter tract having one set of endpoints near the superior parietal cortex and another near the inferior parietal cortex, based on the grey matter ROIs defined by Freesurfer (Desikan et al. 2006; Fischl 2012; see Materials and methods).

Figure 6A shows the group of streamlines that comprises the tract we identified in each hemisphere in six subjects from KU dataset, superimposed on a coronal slice of the T1-weighted anatomical image. The estimated tract, SIPS, primarily connects the superior and inferior parts of the parietal cortex and wraps around the intraparietal sulcus (IPS). In all subjects, SIPS in the two hemispheres are symmetrically oriented. The mean length of the estimated SIPS streamlines was 4.69 cm (SD = 0.59, N = 12 hemispheres). Figure 6B shows the estimated SIPS endpoints on the cortical surface representation in one representative hemisphere (S1, left hemisphere). Most of the dorso-medial SIPS endpoints are in the parietal areas superior to the IPS, but also in the medial areas such as the precuneus. The ventro-lateral endpoints of SIPS are in the supramarginal gyrus, parietal operculum and the posterior end of the lateral sulcus.

Additionally, we analysed the publicly available HCP data (WU-Minn HCP dataset; Van Essen et al. 2013) in order to assess the consistency of SIPS results across datasets. Figure 7A demonstrates SIPS in four subjects from WU-Minn HCP dataset, identified using the identical methods to those used for KU dataset. The estimated position and trajectory of SIPS are consistent with those in KU dataset (Figure 6A).

Figure 7B shows a principal diffusion direction (PDD) map illustrating the position of SIPS in one representative WU-Minn HCP subject (S7). PDD is often used to identify the major white matter tracts, and it allows for tract identification independent of the selection of tractography methods (Pajevic & Pierpaoli 1999; Wakana et al. 2004; Yeatman et al. 2013; Takemura, Rokem, et al. 2016). This PDD map based on WU-Minn HCP dataset clearly shows the existence of a tract travelling between the medial side of superior parietal cortex, and lateral inferior regions around parietal operculum and posterior part of lateral sulcus.

In order to assess the generality of our findings, we analysed dMRI data of 90 subjects from WU-Minn HCP and MGH-USC HCP datasets using a simpler analysis pipeline (see Materials and methods). Figure 8 demonstrates that SIPS was also consistently observed in those subjects. We also describe the population average of the position of SIPS in MNI152 space in Figure 9.

The results of tractography, which is consistent across a large number of subjects and three independent datasets, as well as voxelwise evidence of SIPS that is not based on tractography, further corroborate the evidence for SIPS. Furthermore, SIPS described here is consistent with a short parietal association bundle reported in a series of white matter atlas works (Oishi et al. 2008, 2011; Zhang et al. 2010; Guevara et al. 2017). However, the atlas does not provide additional information regarding the provenance of SIPS; making our study the first to report

the detailed anatomical characteristics of this tract using in vivo dMRI methods and to compare SIPS identified based on in vivo dMRI data to post-mortem findings, as described below.

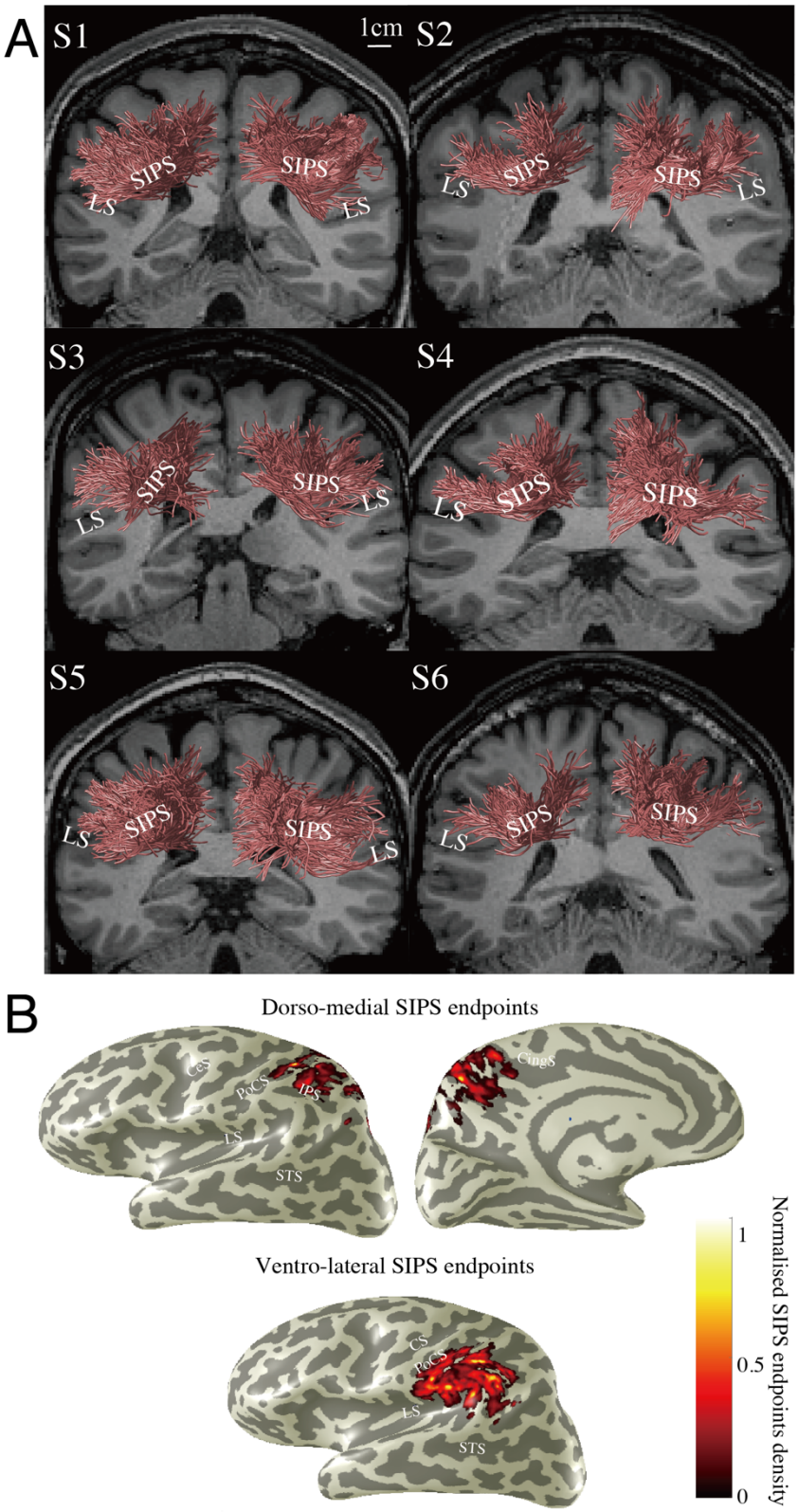
A
S1
1cm
S2
S3
S4
S5
S6
SIPS
LS
B
Dorso-medial SIPS endpoints
CS
PoCS
IPS
LS
STS
CingS
Ventro-lateral SIPS endpoints
CS
PoCS
LS
STS
1
0.5
0
Normalised SIPS endpoints density

Figure 6. Human stratum proprium of interparietal sulcus (SIPS) estimated by tractography performed on dMRI data (KU dataset). A. Coronal view of SIPS (red) in six subjects (S1-S6; KU dataset), identified by tractography (see Materials and methods). Scale bar (white) in the S1 panel indicates 10 mm. The background anatomical (T1-weighted) slice is located immediately anterior to the position of SIPS. LS: Lateral Sulcus. **B.** SIPS endpoints overlaid on the cortical surface (S1, left hemisphere). The spatial distance between SIPS endpoints and grey matter voxels was calculated in order to plot the number of SIPS streamlines having endpoints close to grey matter voxels (see Materials and methods). CS: Central Sulcus, PoCS: Postcentral Sulcus, IPS: Intraparietal Sulcus, STS: Superior Temporal Sulcus, CingS: Cingulate Sulcus.

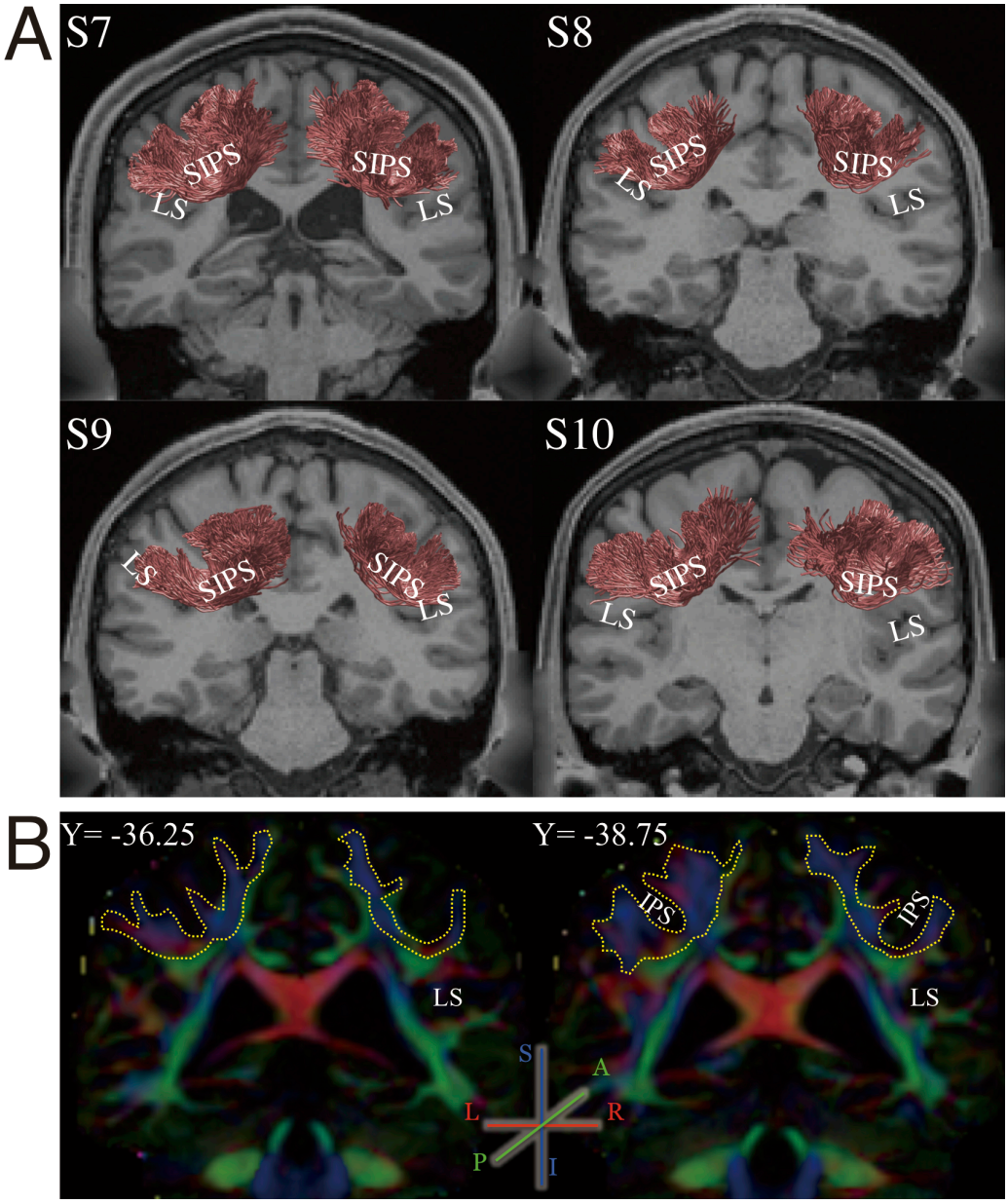

Figure 7. SIPS identified in HCP dataset. A. Coronal view of SIPS (red) in four subjects (S7-S10) from HCP dataset, identified by tractography (see Materials and methods). The conventions are identical to those in Figure 6A. **B.** Position of SIPS highlighted in PDD map (S7, two representative coronal slices; the position of each slice is shown in ACPC coordinate). The colour scheme depicts the PDD in each voxel (blue: superior-inferior; green: anterior-posterior; red: left-right). White matter portion connecting the dorso-medial and ventro-lateral regions wrapping around the intraparietal sulcus (IPS) that is predominantly blue/purple clearly illustrates the trajectory of SIPS. Yellow dotted line highlights the position of SIPS.

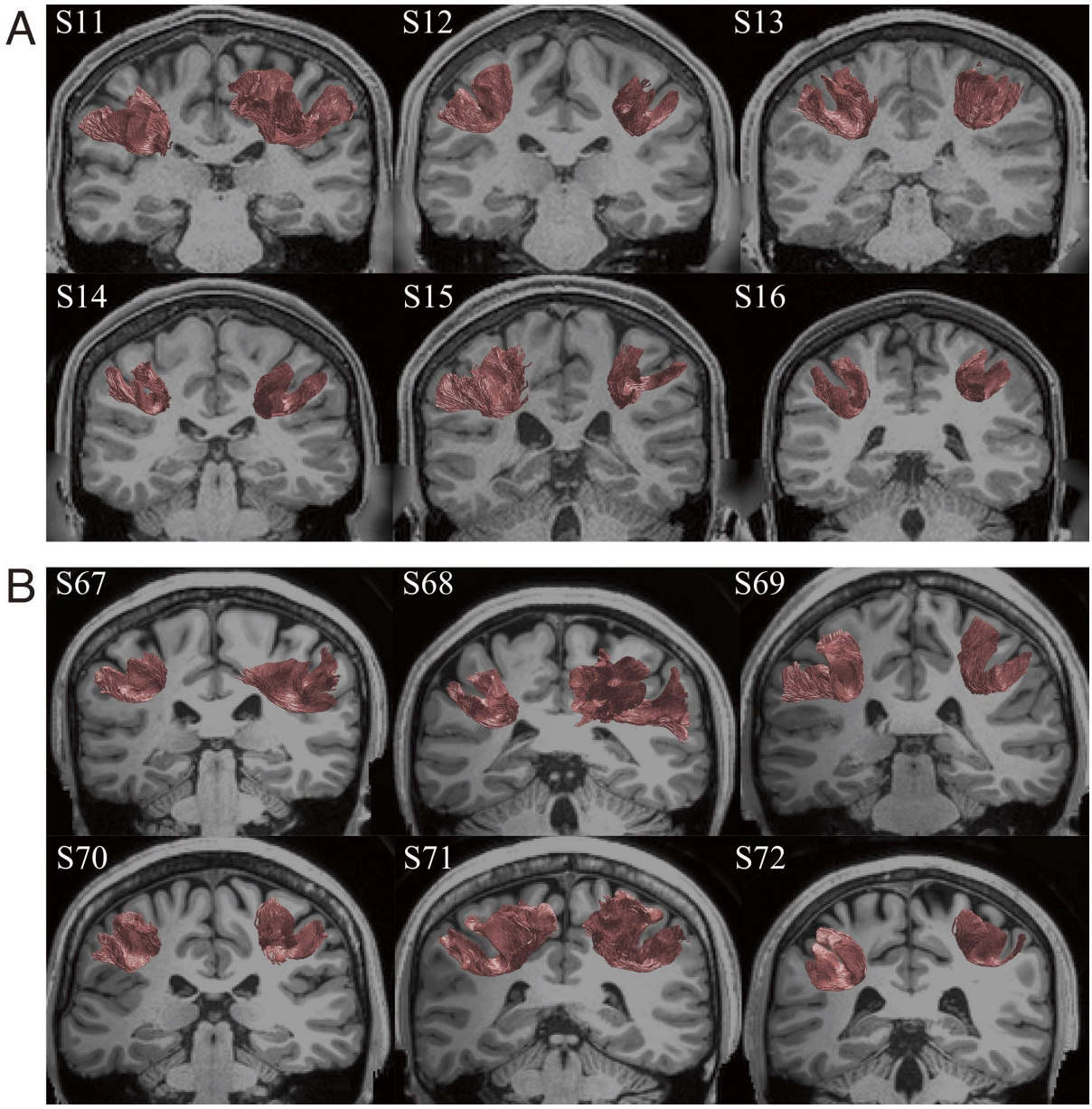

Figure 8. SIPS identified in representative subjects from WU-Minn HCP (A. S11-S16) and MGH-USC HCP (B. S67-S72) datasets. Conventions are identical to those in Figures 2.1 and 2.2.

Sagittal View (Left Hemisphere)

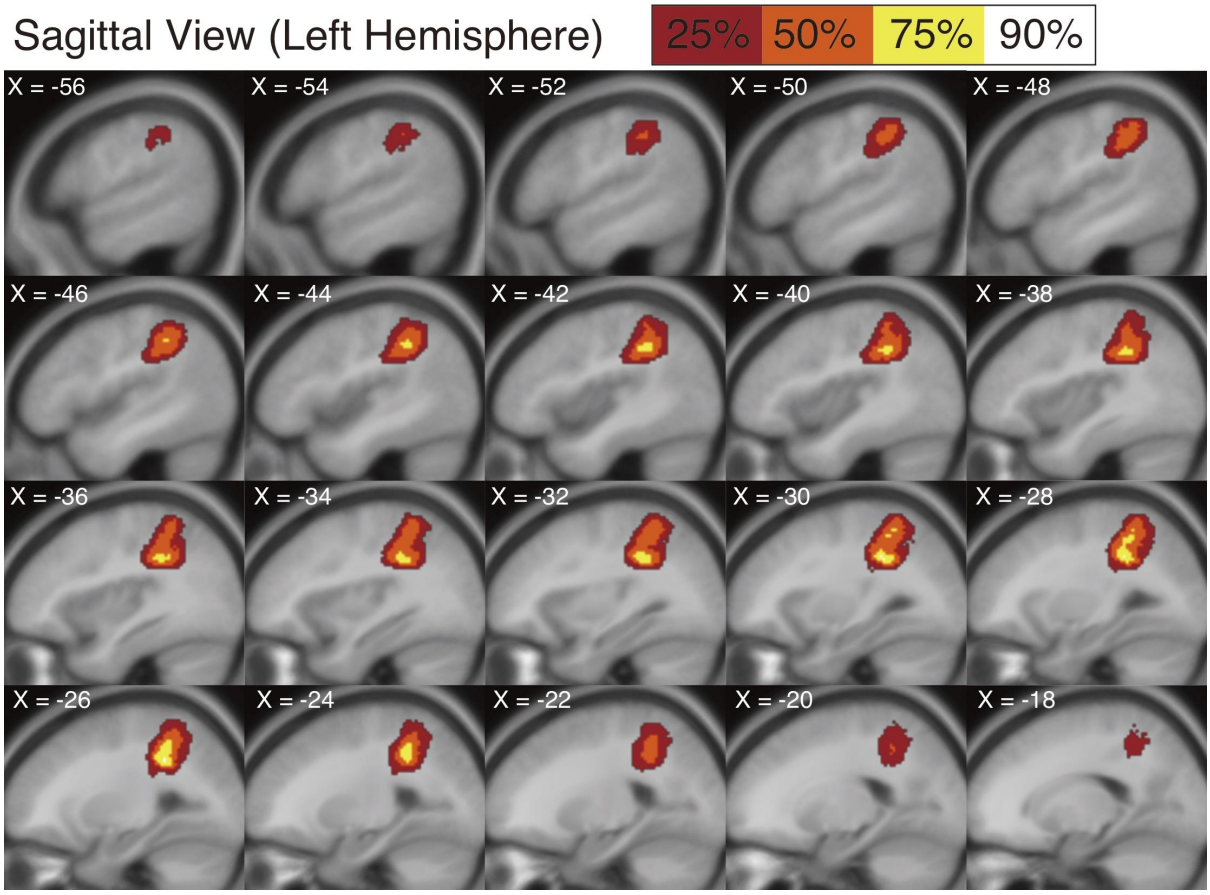

Sagittal View (Right Hemisphere)

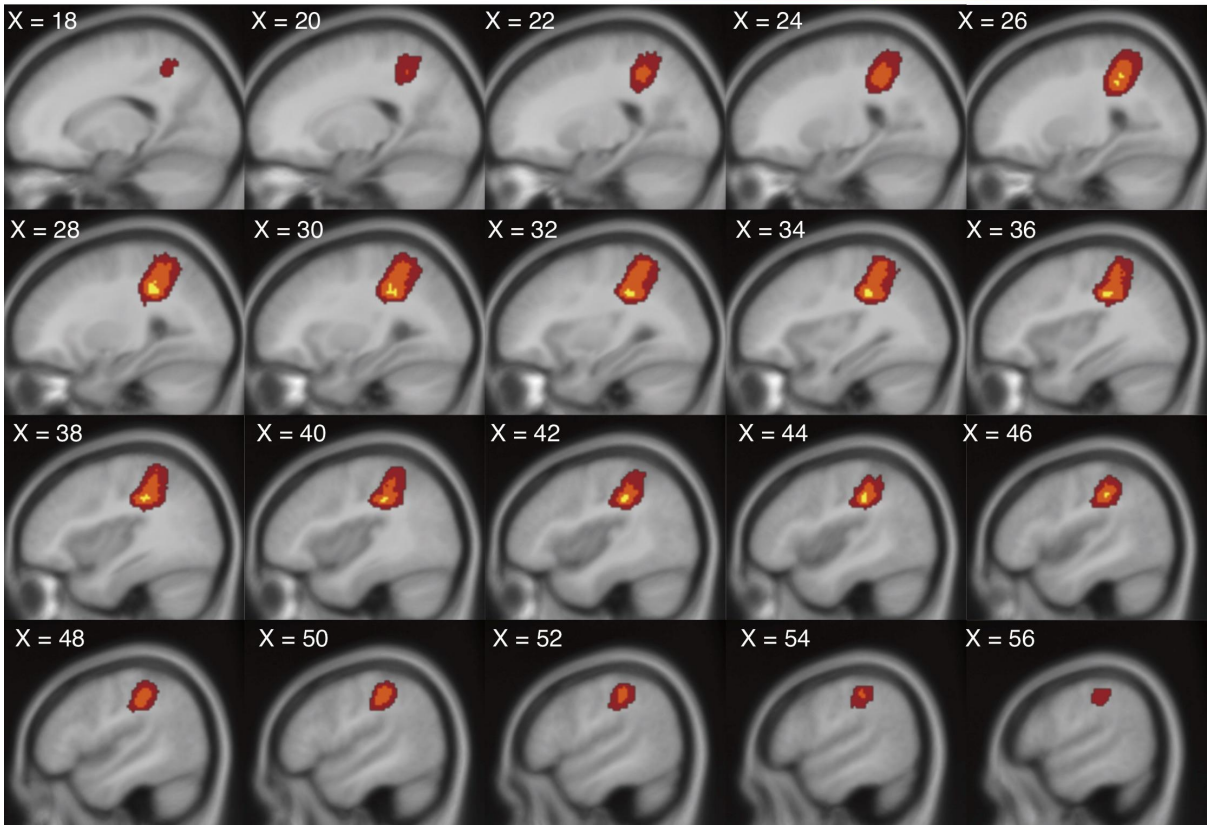

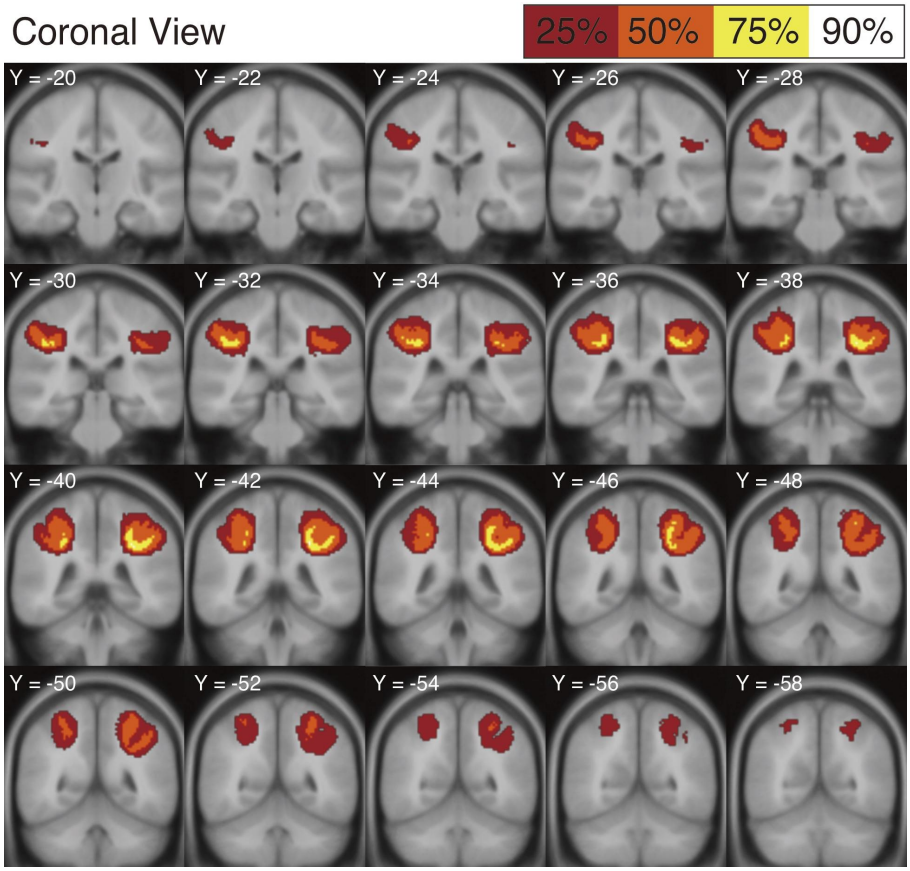
Coronal View
25%
50%
75%
90%
Y = -20
Y = -22
Y = -24
Y = -26
Y = -28
Y = -30
Y = -32
Y = -34
Y = -36
Y = -38
Y = -40
Y = -42
Y = -44
Y = -46
Y = -48
Y = -50
Y = -52
Y = -54
Y = -56
Y = -58

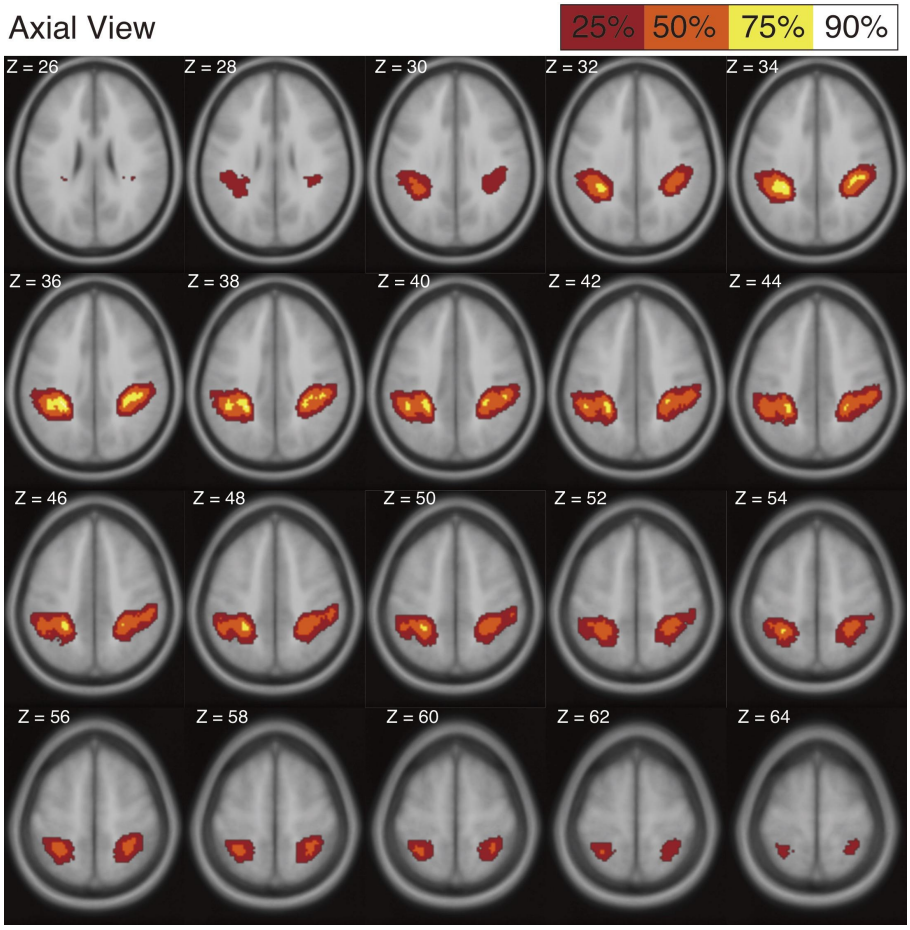
Axial View
25%
50%
75%
90%
Z = 26
Z = 28
Z = 30
Z = 32
Z = 34
Z = 36
Z = 38
Z = 40
Z = 42
Z = 44
Z = 46
Z = 48
Z = 50
Z = 52
Z = 54
Z = 56
Z = 58
Z = 60
Z = 62
Z = 64

Figure 9. Probabilistic population average of 100 subjects in MNI152 space, as shown in sagittal (left hemisphere, right hemisphere), coronal, and axial slices. Colour coding indicates the degree of overlap across subjects. See Materials and methods in the main text for the methods used to create the population atlas.

3.3.1. Comparison with fibre dissection studies

We compared the anatomical position and shape of SIPS identified from dMRI data with post-mortem fibre dissection studies. SIPS has been documented in two previous post-mortem fibre dissection studies; in the classical work by a German neurologist Heinrich Sachs (1892) and more recently by Vergani and colleagues (2014). Sachs referred to this tract as *stratum proprium fissurae interparietalis* in his report, which was later rephrased by Vergani and colleagues (2014) as *stratum proprium of interparietal sulcus* (SIPS). We adopt this term, SIPS, to refer to the tract estimated in the present study.

Figure 10 compares the position of SIPS in Sachs's study (1892; Figure 10A and 10B) and in Vergani's study (2014; Figure 10C), with the tract we identified using tractography (Figure 10D). SIPS identified in this study is consistent with SIPS reported in the fibre dissection studies in several aspects. In terms of its spatial relations with cortical landmarks, SIPS wraps around the intraparietal sulcus, and connects the parietal cortex and the dorsal bank of the lateral sulcus. The position of SIPS on the coronal slice is also consistent. The coronal slice of the anatomical image onto which SIPS estimated by tractography is superimposed in Figure 10D was chosen carefully so that it corresponded with the slices used in the fibre dissection studies as closely as possible. Whilst it is not possible to perfectly match the position of the

slice between our MRI data and fibre dissection studies, it is qualitatively consistent across the four presentations in Figure 10, in terms of the positions of the sulci (i.e. the lateral sulcus and the intraparietal sulcus) and the lateral ventricle. Although SIPS in the three studies cannot be compared quantitatively due to the difference in the methodology used, Figure 10 highlights that the position and trajectory of SIPS identified with our dMRI data agree with those of SIPS reported in the fibre dissection studies.

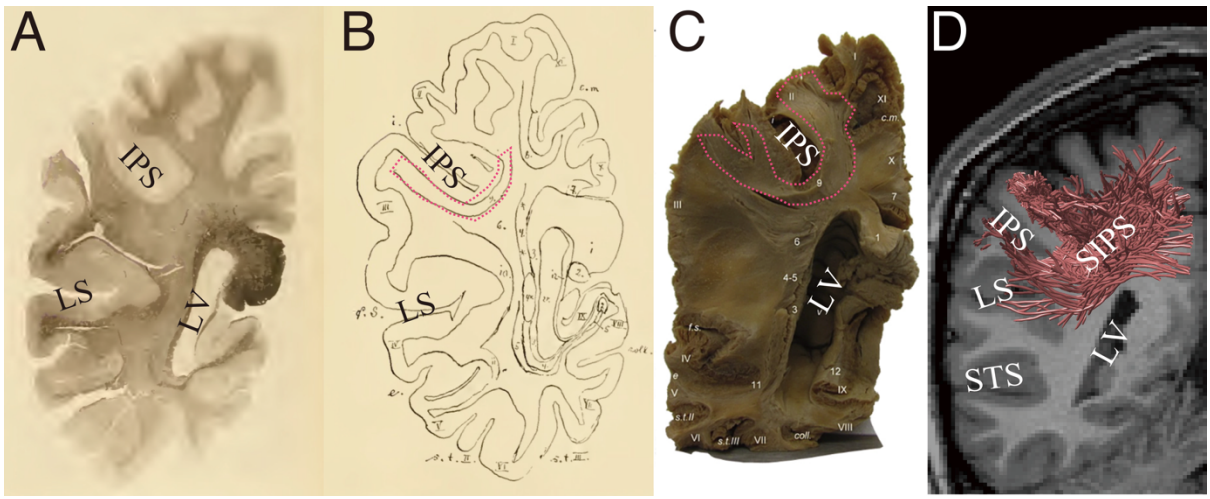

Figure 10. Tractography results are consistent with classical and modern fibre dissection studies. **A.** White matter tract referred to as SIPS on a coronal histological slice and **B.** SIPS (red outline) in the schematic diagram of the fibres visualised in the photo in Panel A (Sachs 1892). Sachs (1892) noted that this slice is approximately 75 mm anterior to the occipital pole (Forkel et al. 2015). **C.** SIPS identified in a post-mortem human brain in the modern fibre dissection study (right hemisphere; Vergani et al. 2014). The position of SIPS is highlighted with red outline. Reproduced from Vergani et al. (2014) with permission. **D.** SIPS estimated by tractography (red lines) in one representative hemisphere (S1; right hemisphere). The image has been flipped (for the original image, see Figure 6A) so that the slice corresponds with the fibre dissection studies. The background coronal slice (ACPC coordinate, Y = -44; approximately 65 mm anterior to the occipital pole) is located immediately anterior to the estimated SIPS. The position and the trajectory of SIPS are qualitatively consistent with those of

SIPS reported in the fibre dissection studies (Panels A-C). LV: Lateral Ventricle, STS: Superior Temporal Suclus, IPS: Intraparietal Sulcus.

3.3.1. Position of SIPS with respect to major white matter tracts

Figure 11 shows SIPS overlaid on a sagittal plane of the T1-weighted image, along with other major white matter tracts reported in previous studies; the arcuate fasciculus (AF; Catani et al. 2002; Wakana et al. 2004), posterior arcuate (pArc; Catani et al. 2005; Weiner et al. 2016) and vertical occipital fasciculus (Yeatman et al. 2013; Yeatman, Weiner, et al. 2014; Duan et al. 2015; Takemura, Rokem, et al. 2016) in one representative subject (S1).

SIPS is located adjacent to AF; in fact, SIPS intersects with the dorsal surface of AF. This crossing may be one of the reasons that this tract has been relatively neglected in the literature, as resolving crossing fibres is one of the critical limitations of the diffusion tensor-based approach (Frank 2001; Tournier et al. 2012). Interestingly, the intersection between SIPS and AF may explain the pattern of previous dMRI results along AF. Yeatman & colleagues (2011) investigated the fractional anisotropy (FA; Basser & Pierpaoli 1996) along AF, and found that there is a large dip in the FA value along the length of the fasciculus in the vicinity of the temporal cortex. Yeatman et al. (2011) suggests that this dip is partially accounted for by the sharp curvature of AF, but also by partial voluming with crossing fibres. Since the location of this dip along the trajectory of AF coincides with the position of SIPS, it seems plausible that this is where AF intersects with SIPS.

SIPS is also located near pArc, but the trajectory and endpoints of SIPS are distinct from pArc, which connects the parietal cortex and the anterior inferior temporal cortex.

Although there are a few neighbouring tracts, some of which cross or kiss SIPS, the differences in the trajectory and locations of endpoints between those known tracts and SIPS clarify that SIPS is a distinct tract.

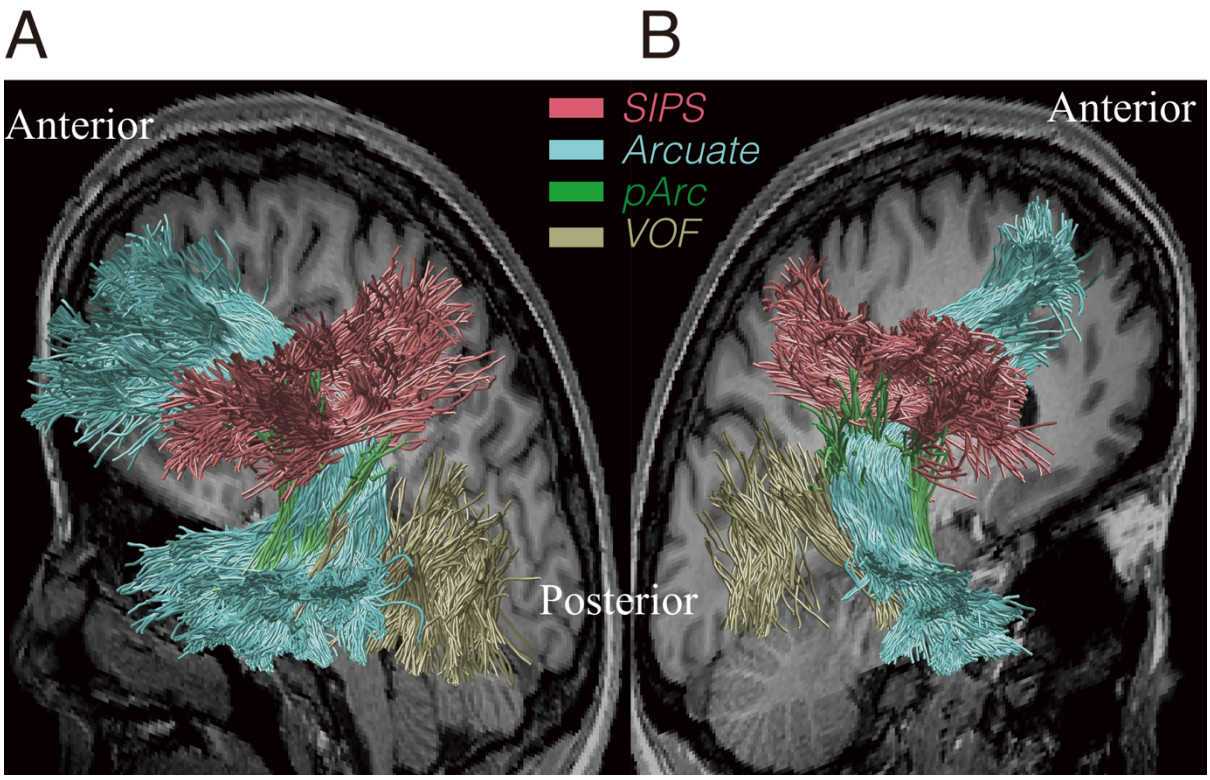

Figure 11. Position of SIPS with respect to other tracts. A. Position of SIPS with respect to other tracts in the left hemisphere of one representative subject (S1). The background T1-weighted image is a sagittal slice in the medial portion of the brain. SIPS (red) is located superior to the vertical occipital fasciculus (VOF; yellow) and posterior arcuate (pArc; green). SIPS lies on the superior surface of, and crosses with the arcuate fasciculus (Arcuate; light blue). **B.** Position of SIPS with respect to other tracts in the right hemisphere in the same subject (S1).

3.2. Statistical evidence in support of SIPS

To evaluate the strength of statistical evidence supporting the existence of SIPS, we used the virtual lesion methods (Honey & Sporns 2008; Pestilli et al. 2014; Leong et al. 2016; Takemura, Rokem, et al. 2016). We first computed the cross-validated prediction accuracy for diffusion signals (R_{rmse}; Rokem et al. 2015; Takemura, Caiafa, et al. 2016) in models with lesioned and unlesioned SIPS. We then compared the distribution of R_{rmse} of the two models to predict the diffusion signals within SIPS voxels (see Materials and methods for details). We quantify the strength of evidence (S) in support of the SIPS by calculating the difference of R_{rmse} in lesioned and unlesioned models divided by the standard deviation of the R_{rmse} (Pestilli et al., 2014).

Figure 11A describes the mean and variance of the statistical evidence for SIPS across subjects, yielded by the virtual lesion analysis. The mean strength of statistical evidence for SIPS was S = 76.25 (SD = 10.87) for the left hemisphere, and S = 84.7 (SD = 6.72) for the right hemisphere. Figure 11B describes the two-dimensional histogram of R_{rmse} in the SIPS lesioned and unlesioned models for the left hemisphere in one representative subject (S1). In many voxels, the SIPS lesioned model showed substantially lower model accuracy (higher R_{rmse}) as compared with the unlesioned model, indicating that SIPS is necessary to explain the diffusion signals within those voxels. Thus, in addition to the results of tractography and their consistency with the findings of previous post-mortem studies at visual inspection, there is strong statistical evidence supporting the existence of SIPS.

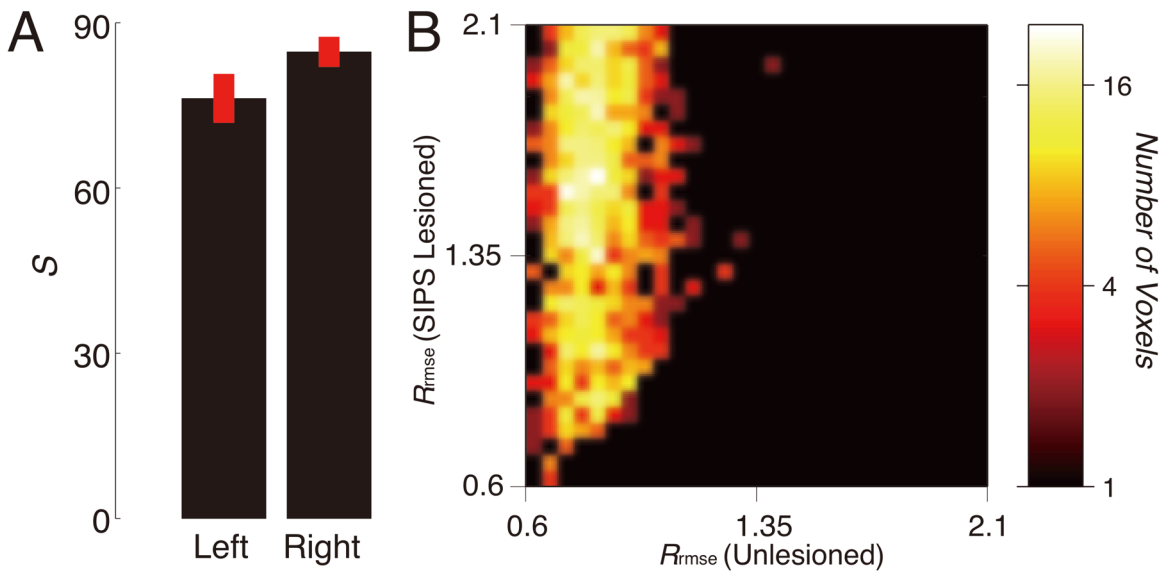

Figure 12. Statistical evidence in support of SIPS. A. Mean *S* in support of left and right SIPS across subjects. Error bars depict ±1 s.e.m across subjects. **B.** Two-dimensional histogram comparing the model accuracy (R_{rmse}) between the lesioned and unlesioned models (horizontal axis: unlesioned model; vertical axis: lesioned model) for SIPS in the left hemisphere in one representative subject (S1). Prediction accuracy is substantially lower with the lesioned model. Colour bar (right panel) indicates the number of voxels.

3.3. SIPS and its relations with optic-flow selective cortical areas

With the subjects in KU dataset, we further conducted fMRI experiments to localise cortical sensory areas selective for optic-flow stimulation in order to examine the spatial proximity between the SIPS endpoints and those functionally-defined areas.

3.3.1. Functional localisation

To localise the cortical areas selective for optic-flow stimulus, blood-oxygen level dependent (BOLD) responses to the coherent optic-flow stimulus was contrasted against those to the random-motion stimulus. We identified four of the cortical areas known to be selective for optic flow (Figure 13; VIP, p2v, PcM, PIC+; Cardin & Smith 2011; Uesaki & Ashida 2015). Areas VIP, p2V and PcM are located in the superior part of the parietal cortex, and PIC+ in the posterior end of the lateral sulcus. The locations of those areas in Talairach coordinates were consistent with those of the corresponding areas reported in previous studies (Cardin & Smith 2011; Frank et al. 2014; Uesaki & Ashida 2015). All four areas were successfully identified in nine hemispheres. In the other three hemispheres, either PcM or VIP was not identified.

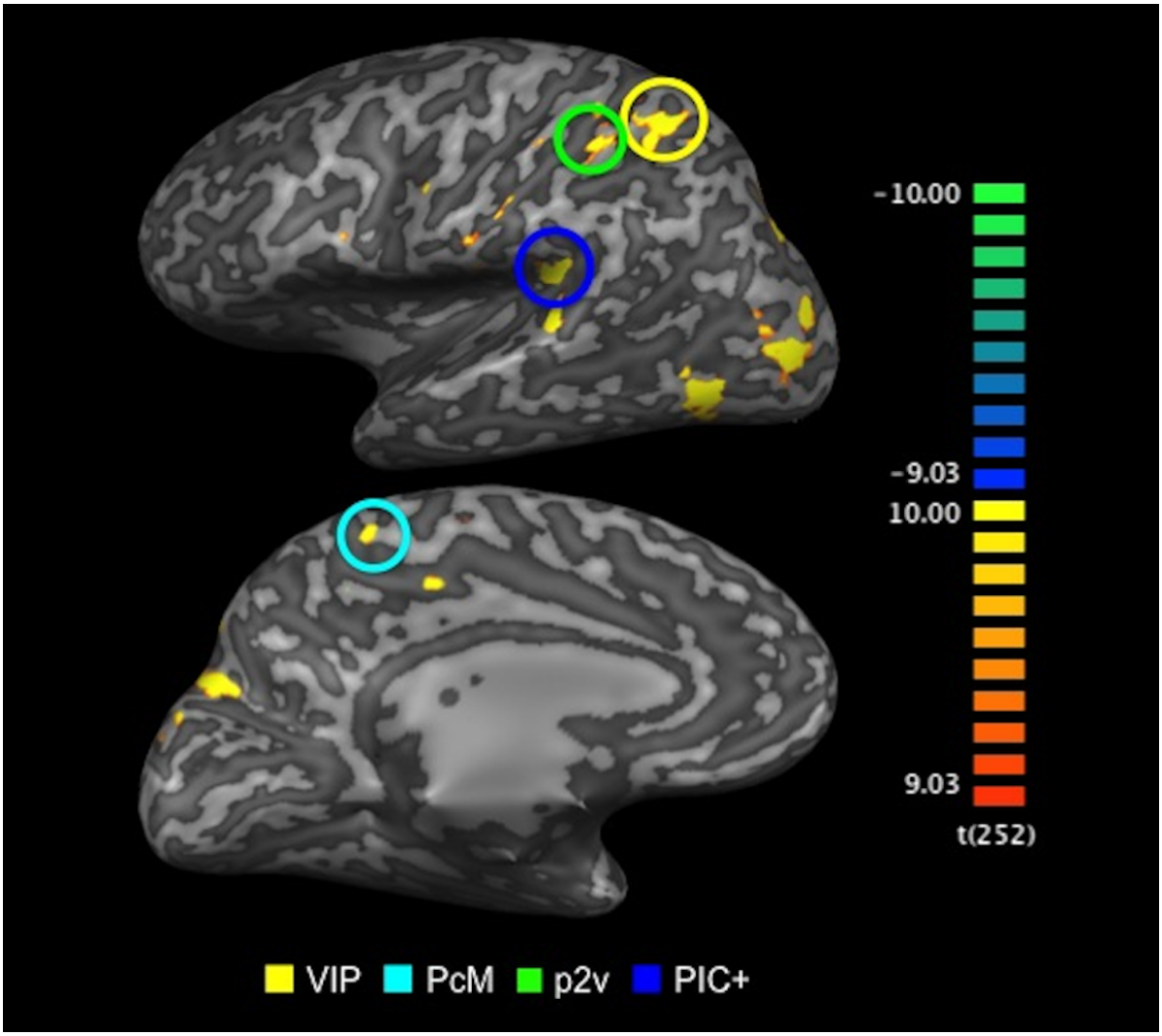

Figure 13. Optic-flow selective areas localised using fMRI. Cortical areas that showed significantly greater BOLD responses to optic-flow stimulus than to random-motion stimulus ($p < .005$, uncorrected). Activation maps are superimposed on the inflated cortical surface of the left hemisphere in one representative subject (S1). Colour-coded bar (right panel) indicates statistical t-values (degree of freedom indicated in brackets). Four of the cortical areas selective for optic flow (VIP, PcM, p2v and PIC+) were successfully identified.

3.3.2. SIPS endpoints and optic-flow selective cortical areas

Subsequently, we examined the spatial proximity between the cortical areas selective for optic flow (Figure 13) and the SIPS endpoints. Although there is a limitation to use tractography for identifying the tract endpoints in the grey matter (Reveley et al. 2015), it is still useful to understand how closely functionally-defined ROIs are located to the tract endpoints in order to infer any potential implication of the tract in information transmission during optic-flow processing. We analysed the general spatial proximity between the SIPS endpoints and the optic-flow selective areas (VIP, PcM, p2v and PIC+).

Figure 14A depicts the relative position of SIPS with respect to the cortical areas selective for optic flow, in the left hemisphere of one representative subject (S1; see Figure 15 for other examples). PIC+ is located in the posterior end of the lateral sulcus, near the ventro-lateral endpoints of SIPS. Three of the optic-flow selective areas (VIP, p2v and PcM) in the parietal cortex are located near the dorso-medial endpoints of SIPS. Whilst the ventro-lateral endpoints are observed in the vicinity of PIC+ in a consistent manner across hemispheres, there are some degrees of variability in the spatial proximity between the superior parietal ROIs and dorso-medial endpoints of SIPS across hemispheres (Figure 15). This variability may be due to the limitation of tractography in identifying the exact tract endpoints near smaller cortical regions located in the gyrus walls (Reveley et al., 2015). Figure 14B summarises the proportion of grey matter voxels in each optic-flow selective area located near the SIPS endpoints (see Materials and methods). Approximately 40 and 80% of voxels in each grey matter ROI are located in the vicinity of the SIPS endpoints, depending on the distance threshold for defining the spatial proximity between the grey matter voxels and tract endpoints (i.e. proximity was thresholded at 3 mm or 4.5 mm). It seems highly likely that SIPS is part of the anatomical connection

between the optic-flow selective areas in the superior parietal cortex (VIP, p2v and PcM) and the PIC+.

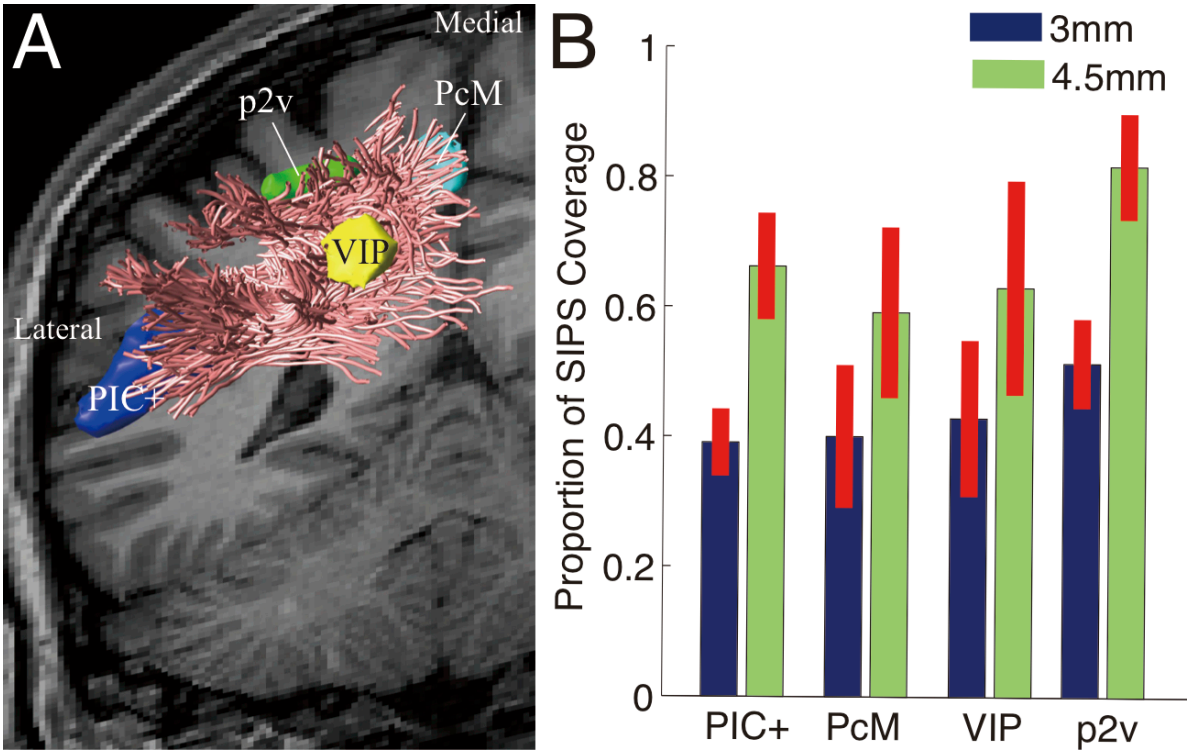

Figure 14. Spatial proximity between SIPS endpoints and cortical ROIs selective for optic-flow stimulation. A. Position of SIPS (magenta lines) in relation to the cortical ROIs identified by optic-flow stimulation using fMRI (dark blue: PIC+; light blue: PcM; yellow: VIP; green: p2v) in the left hemisphere in one representative subject (S1). **B.** SIPS map coverage across all hemispheres. Vertical axis represents the proportion of voxels in each ROI within 3 mm (blue) and 4.5 mm (green) from SIPS endpoints. Error bars indicate ± 1 s.e.m. across hemispheres.

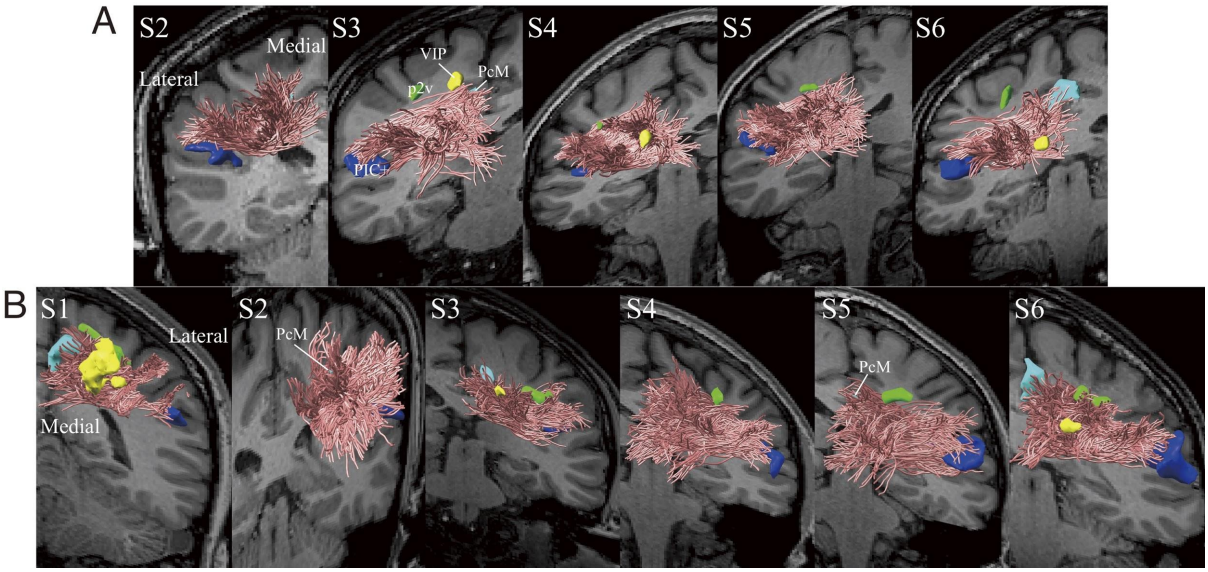

Figure 15. Spatial proximity between SIPS endpoints and optic-flow selective cortical ROIs in remaining 11 hemispheres (A. left hemispheres; B. right hemispheres). While the ventro-lateral endpoints of SIPS are consistently located adjacent to PIC+, there is some variability in the spatial relations between the parietal ROIs (PcM, VIP and p2v) and the dorso-medial SIPS endpoints across hemispheres. Conventions are identical to those in Figure 14.

4. Discussion

Stratum proprium of interparietal sulcus (SIPS) was originally discovered in a post-mortem fibre dissection study by Sachs (1892) and was reproduced in another post-mortem study by Vergani et al. (2014). Here, SIPS was successfully identified in the living human brain, using dMRI and tractography.

4.1. Comparison of SIPS results with anatomical studies

In this study, we investigated a white matter tract that has been largely overlooked in the visual and cognitive neuroscience, SIPS, using dMRI-based tractography and fascicle evaluation techniques. In spite of the challenges of using tractography to study the little-investigated white matter tract, SIPS was consistently identified across subjects and datasets. Between our dMRI results and the findings of the following anatomical studies, there is converging evidence supporting the existence of SIPS.

4.1.1. Human post-mortem fibre dissection studies

Most importantly, our results are consistent with human post-mortem fibre dissection studies (Figure 10; Sachs 1892; Vergani et al. 2014). In those studies, SIPS was found to be located immediately posterior to the central sulcus, wrapping around the intraparietal sulcus, and to range between the superior parietal cortex and the lateral fissure. The position and the trajectory of SIPS reported in the post-mortem fibre dissection studies are consistent with those of SIPS identified in vivo in three independent dMRI datasets in this study (Figures 1-4).

To our knowledge, the first description of SIPS appeared in the atlas by Heinrich Sachs (1892); a German neurologist and neuroanatomist who studied under Wernicke. Sachs's atlas (1892) describes the white matter tracts in the post-mortem human brain in great detail, including the U-fibre system which has not been studied extensively in the living human brain. One of the short-association tracts described is a tract termed *stratum proprium fissurae interparietalis*. Despite its relevance to perceptual and cognitive neuroscience, Sachs's atlas has been largely overlooked in the literature partly due to the lack of translation of the atlas from German to

English (see Forkel et al. 2015; for a historical review and English translation of the atlas). SIPS documented in this classical atlas was recently reproduced in a modern fibre dissection study by Vergani and colleagues (2014).

Our results describe the characteristics of SIPS identified in the living human brain, using modern neuroimaging techniques, which are highly consistent with the findings of the human post-mortem studies; hence providing further evidence for SIPS.

4.1.2. Macaque tracer study

Additionally, we note that a tract similar to human SIPS in the macaque brain has been reported in a tracer study. In their extensive study, Schmahmann and Pandya (2006) injected retrograde tracers into the macaque brain, and inspected the trajectory of white matter tracts from the injection sites. They reported several major white matter tracts seemingly homologous to human major white matter tracts identified in dissection studies (such as the inferior longitudinal fasciculus, and the superior longitudinal fasciculus); and those findings were later substantiated by macaque dMRI results (Schmahmann et al. 2007). In addition to the major white matter tracts, Schmahmann and Pandya (2006) also reported a fibre bundle wrapping around the intraparietal sulcus. They note (page 120):

> *A dorsal fiber bundle lies subjacent to the cortex of the lower bank of the IPS and terminates in a columnar manner in area POa and in area IPd (Scs. 105, 113). These fibers continue medially and then curve around the depth of the IPS to ascend in the white matter of the superior parietal lobule. They terminate in area I in a columnar manner and then first layers of area 3b and 3a in the caudal bank and depth of the*

central sulcus (Sc. 105). Further caudally, these medially directed fibers terminate in a columnar manner in area 2 (Sc. 113).

Because of the compelling similarity between this fibre bundle identified in the macaque brain and human SIPS in terms of their anatomical positions and shapes, it could be hypothesised that this fibre bundle in macaque may be the homologue of human SIPS identified in this study.

Whilst the white matter structure of the macaque brain may be different from that of the human brain to some extent (Rilling et al. 2008), the fact that there is a white matter tract in the macaque brain that largely resembles human SIPS is encouraging for future investigations on human-macaque homology with respect to SIPS. There is a growing trend in neuroanatomy to use dMRI methods to compare the macro-scale white matter anatomy of the human brain and that of the macaque brain (Schmahmann et al. 2007; Oishi et al. 2011; Thiebaut de Schotten et al. 2011; Jbabdi et al. 2013; Mars et al. 2015; Takemura et al. 2017), which complements studies that investigate human-macaque homology of cortical maps using fMRI (Brewer et al. 2002; Tsao et al. 2003, 2008; Wade et al. 2008; Goda et al. 2014; Kolster et al. 2014). It will be beneficial to study the precise anatomy of SIPS both in humans and macaques, in order to integrate the insights from macaque electrophysiology as well as tracer studies (Thiebaut de Schotten et al. 2012), and human fMRI studies investigating the neuronal network for multisensory integration guiding self-motion perception.

4.2. Functional localisation of optic-flow selective sensory regions

Recent fMRI studies have shown that the sensory areas in the superior parietal regions (VIP, PcM, p2v) as well as an area around the posterior end of the lateral sulcus and parietal

operculum (PIC+) are activated by optic-flow stimulation (Wall & Smith, 2008; Cardin & Smith 2011; Greenlee et al. 2016). As in Chapter 2, this study employed the functional localiser based on that described in Pitzalis et al. (2010), in order to identify VIP, PcM, p2v and PIC+. The locations of those regions are consistent with those of the counterparts reported in previous studies (Cardin & Smith 2011; Uesaki & Ashida, 2015).

We note that the definition and terminology of the area referred as PIC+ in this study have been debated in the literature. In some earlier publications (Wall & Smith 2008; Cardin & Smith 2010, 2011; Uesaki & Ashida 2015), an area identified using optic-flow localisers was referred to as the parieto-insular vestibular cortex (PIVC) and was considered to be involved in integrating visual and vestibular information to guide self-motion perception. However, a recent vestibular fMRI study showed that PIVC is selectively responsive to vestibular stimulation, and is unlikely to be activated by visual stimulation (Frank et al. 2016; Greenlee et al. 2016). Frank and colleagues (2014) also suggested that PIVC and the area activated by visual stimulation, which is referred to as "PIC" in their study, are two independent areas. Their findings show that PIVC is purely vestibular, whilst PIC is predominantly visual but also processes vestibular information. Here, we use "PIC+" to refer to the area around the posterior end of the lateral sulcus and parietal operculum, activated during optic-flow stimulation, as we did not examine the responsiveness of the area to vestibular stimuli.

Results suggest that the ventro-lateral endpoints of SIPS are near PIC+ (Figure 7), but it is unclear whether these endpoints are also located near PIVC identified in vestibular fMRI studies (Frank & Greenlee 2014; Frank et al. 2014; Greenlee et al. 2016). Considering the proximity between PIC and PIVC (Frank & Greenlee 2014; Frank et al. 2014; Greenlee et al. 2016), it is possible that the ventro-lateral endpoints of SIPS are also adjacent to PIVC. Future

studies should assess whether PIVC is directly connected to the superior part of the parietal cortex through SIPS, or indirectly connected via short-range connections with PIC+, in order to construct a more comprehensive model to understand how visual and vestibular signals are transmitted between these areas to guide self-motion perception.

4.3. SIPS and its implication in visuo-vestibular integration

Optic flow is a moving pattern on the retina caused by the relative motion between the observer and the scene, and is one of the most important visual cues to the estimation of self-motion (Gibson 1950, 1954; Warren & Hannon 1988). However, in most cases, perception of self-motion depends on integration of optic-flow information and signals from other sensory modalities such as the vestibular system. In order to understand the neuronal mechanism involved in the estimation of self-motion, it is important to elucidate how the visual and vestibular signals are integrated when we observe optic flow. Previous fMRI studies investigating the cortical areas selective for optic-flow and vestibular stimuli suggest that the sensory areas in the parietal cortex are involved in visuo-vestibular integration necessary for self-motion estimation (Wall & Smith 2008; Cardin & Smith 2011; Greenlee et al. 2016). Yet, the white matter anatomy that supports the communication amongst those areas has received very little attention in the literature of visual and cognitive neuroscience, even though the existence of SIPS has been known for over a century (Sachs 1892; Vergani et al. 2014).

One of the biggest advantages of the dMRI-based approach is that the positions of estimated white matter tracts and functionally localised cortical areas can be compared in the brain of the same individual. This is particularly important in order to hypothesise the types of information that are transferred via the tracts of interest (Kim et al. 2006; Greenberg et al. 2012; Yeatman

et al. 2013; Takemura, Rokem et al. 2016; Rokem et al. 2017). We combined dMRI and fMRI, and analysed the spatial proximity between the SIPS endpoints and the optic-flow selective cortical areas localised within the same subjects. Results show that the dorso-medial SIPS endpoints are near VIP, PcM and p2v, and the ventro-lateral SIPS endpoints near PIC+, despite some variability in the spatial proximity between the superior parietal ROIs and dorso-medial endpoints of SIPS across hemispheres (Figure 14 and 2.10). These cortical areas have been associated with the convergence of visual and vestibular information regarding self-motion (Fetsch et al. 2009; Prsa et al. 2012; Uesaki & Ashida 2015; Kleinschmidt et al. 2002; Kovacs et al. 2008; Wiest et al. 2004; Butler et al. 2010). Our results and those findings together suggest that communication between VIP, PcM, p2v and PIC+ likely plays a crucial role in multisensory integration necessary for accurate perception of self-motion, and that it is supported by SIPS. The spatial relationship between SIPS and the optic-flow selective areas will have implications for interpreting the consequence of white matter lesions that include SIPS, or exploring the neuronal basis of individual difference in self-motion perception.

4.4. Limitations and directions for future research

Our findings show that SIPS is an important structure supporting communication amongst sensory areas in the parietal cortex. It must be noted, however, that it is possible that our results represent only a subset of SIPS. Our tractography results are based on in vivo dMRI data with 1.25 to 2 mm isotropic spatial resolution, but LiFE analysis generally supports larger portions of fibre tracts as the data resolution improves (Pestilli et al. 2014; Takemura et al. 2017). Tractography based on data with higher resolutions would likely allow for the extraction of a larger portion of SIPS. Likewise, estimation of cortical endpoints would be more accurate with

data of better quality, as some cortical endpoints are still missed even with the best dMRI data currently attainable (Reveley et al. 2015).

Other limitations that should be considered include the lower b-value (1000 s/mm^2) used in the acquisition of KU dataset. It has been suggested that lower b-values are not optimal for resolving crossing fibres (Tournier et al. 2004; Alexander & Barker 2005), despite their relatively higher signal to noise ratio. In order to compensate for this limitation, we included HCP data acquired with higher b-values, higher spatial and angular resolution from a large number of subjects. Results demonstrated the compelling consistency in the tractography results across the three datasets. This approach complements the relative disadvantage of the current version of LiFE that it only accepts single-shell data. Contrary to the single-shell approach, multi-shell approaches can be used to generate alternative matrices, which provide additional information regarding tissue microstructures that cannot be captured at a voxel level using single-shell approaches.

It should also be noted that, although SIPS is discussed mainly within the contexts of multisensory integration and optic-flow processing in this article, the SIPS endpoints appear to be near the cortical areas involved in other cognitive functions such as attention (Corbetta & Shulman 2002; Yantis et al. 2002; Bisley & Goldberg 2003), memory (Cabeza et al. 2008; Koenigs et al. 2009; Uncapher & Wagner 2009; Chun & Johnson 2011), motor sequence learning (Rizzolatti & Luppino 2001), visuomotor control (Culham et al. 2006), decision making (Platt & Glimcher 1999), body-ownership (Blanke 2012) and social cognition (Decety & Lamm, 2007). In order to further understand the implications of SIPS in relation to human behaviour, it may be useful to test the relationship between individual differences in diffusion properties along SIPS (e.g. FA) and behavioural measures, as has been done for other white

matter tracts in previous studies (Genç et al. 2011; Yeatman et al. 2012a; Tavor et al. 2014; Gomez et al. 2015; Leong et al. 2016).

On the other hand, for relatively small tracts like SIPS, especially if they cross or kiss other major tracts like AF (Figure 3), it is difficult to interpret the results regarding diffusion properties derived from diffusion tensor-based analyses. Possible solutions to these limitations include acquiring dMRI data at a higher angular resolution with multiple b-values, use of other dMRI techniques (e.g. neurite orientation dispersion and density imaging; NODDI; Zhang et al. 2012), and combining dMRI data with quantitative MRI measurements, to evaluate the physical properties of SIPS in a manner relatively independent from fibre crossings (Dell'Acqua et al. 2013; Mezer et al. 2013; Yeatman et al. 2014b; Mohammadi et al. 2015; Stikov et al. 2015; Weiskopf et al. 2015). Future dMRI studies should examine the properties of SIPS in relation to cognitive functions, as well as development and diseases, with consideration to shortcomings of currently available MRI techniques. In order to facilitate further research on SIPS, we describe the methods and provide open-source implementations (https://github.com/htakemur/SIPS; https://github.com/yeatmanlab/AFQ).

5. Conclusion

This study identified a white matter tract, SIPS, in the living human brain using dMRI and tractography. It is located immediately posterior to the central sulcus and around the intraparietal sulcus; and connects the superior and inferior parts of the parietal cortex. The location and the trajectory of SIPS are consistent with those observed in post-mortem fibre dissection studies by Sachs (1892) and Vergani et al. (2014). SIPS was identified consistently

across a large number of subjects from three independent dMRI datasets, and the existence of the tract was further corroborated by statistical evidence. These findings place SIPS in a good position to channel neuronal communication between the distant cortical areas underlying visuo-vestibular integration necessary for optic-flow processing and perception of self-motion. In vivo identification and characterisation of SIPS using dMRI data and tractography will open new avenues to further studying this tract in relation to diseases, development and brain functions.

Chapter 4: General discussion

The work included here has investigated the anatomical mechanisms for processing optic flow as a cue to self-motion.

Optic flow is one of the most important sensory cues to estimating the observer's relative position, orientation and displacement in the environment, thus supporting perception of self-motion and successful navigation through the environment. Human observers are able to perceive and extract information such as direction of heading (Gibson 1950; Lappe et al. 1999; Warren & Hannon 1988; Furlan et al. 2013), time to contact (Lee 1980), distance travelled (Redlick et al. 2001), segmentation of object motion (Logan & Duffy 2006; Warren & Rushton 2008), and the slant of surfaces in the scene (Koenderink 1986), from optic flow.

However, self-motion perception based solely on optic flow maybe error-prone. For example, because optic flow can only provide heading information in the coordinates of the eyes, which move relative to the head and therefore the body. In order for the whole-body heading to be established, information regarding movement of the head as well as the body has to be factored in (Lappe et al. 1999). Another limit of optic flow is that it is almost always accompanied by the retinal motion due to the movement of the objects in the environment. For accurate perception of self-motion, these different sources of motion have to be parsed (Warren & Rushton 2009). Because the reliability of optic flow in the computation of self-motion is variable, perception of self-motion is constructed based on a multitude of different sensory systems such vestibular system that provides complimentary information (Alais & Burr 2004; Butler et al. 2010; Ernst & Banks 2002; Knill & Saunders 2003). When the sensory systems

receive inputs during self-motion, these inputs are evaluated, weighted and integrated according to their reliability (Fetsch et al. 2012). This sensory integration indicates the involvement of polysensory areas.

Recent imaging studies have identified a number of cortical areas that are responsive to optic flow, which are thought to underlie the ability to accurately perceive self-motion. These areas include the middle temporal complex (MT+; Annese et al. 2005; Dumoulin et al. 2000; van Essen et al. 1981), V6 in the parieto-occipital sulcus (Dukelow et al. 2001; Morrone et al. 2000; Wall & Smith 2008; Cardin & Smith 2010, 2011; Pitzalis et al. 2010; Furlan et al. 2013), the ventral intraparietal area (VIP; Felleman & van Essen 1991; Andersen et al. 1990; Tanaka & Saito 1989; Duffy & Wurts 1991; Schaafsma & Duysens 1996; Cardin & Smith 2010, 2011), the putative area 2v (p2v; Guldin & Grusser 1998; Cardin & Smith 2010, 2011), the cingulate sulcus visual area (CSv; Wall & Smith 2008; Cardin & Smith 2010, 2011; Smith et al. 2017) and the region of the precuneus dorsal to the ascending arm of the cingulate sulcus (precuneus motion area; PcM; Wall & Smith, 2008; Cardin & Smith, 2010, 2011), the posterior-insular complex (PIC+: Deutschländer et al. 2004; Cardin & Smith 2010, 2011; Biagi et al. 2015; Uesaki & Ashida 2015; Wada et al. 2016; Frank et al. 2014; Frank et al. 2016; Greenlee et al. 2016).

Whilst the existence of these areas is well-established, whether optic flow is encoded differentially in these areas when it is processed as a by-product of the observer's self-motion remains unclear. Since perception of self-motion is a multisensory process (Wertheim, 1994; Wexler et al., 2001), the primary aims of this thesis were:

1. Which of the areas selective for optic flow are pivotal in sensory integration underlying self-motion perception?
2. How do those distant areas channel sensory signals to each other through the white matter?

To this end, a series of neuroimaging experiments were conducted to address these questions.

1. Polysensory areas VIP and PIC+ integrate visual and vestibular signals

Chapter 2 employed fMRI and behavioural measurement to identify optic-flow selective areas that are involved in the processing of visual cues to self-motion. By introducing an illusory sensation of self-motion as an index, we assessed which of the optic-flow selective areas reflected the sensation of self-motion. It was concluded that in visual areas MT+, V6, and polysensory areas VIP, PIC+ encoded optic flow differentially depending on whether perception of optic flow was accompanied by sensation of self-motion. It was inferred that the polysensory areas VIP and PIC+ in the parietal cortex may be the loci of visuo-vestibular integration underlying perception of optic flow and self-motion. The findings also indicated that activity in the optic-flow selective visual areas MT+ and V6 was modulated by the feedback from those polysensory areas.

2. SIPS supports signal transmission between polysensory optic-flow selective areas

In light of those results, Chapter 3 aimed to identify a white matter tract connecting the superior part of the parietal cortex in the proximity of VIP, and the inferior part of the parietal cortex in

the proximity of PIC+, which support interaction between these areas underlying visuo-vestibular interaction necessary for perception of optic flow and self-motion. In order to investigate the spatial relations between the optic-flow selective areas and the white matter tract, the experiment was conducted using fMRI and dMRI in conjunction with tractography, in the same set of subjects. In spite of the technical challenges discussed, the white matter tract linking the superior and inferior parts of the parietal cortex was identified successfully in all subjects, including additional subjects sampled from the publicly available datasets. It was found that this tract coincided with SIPS that was first documented in the report of a post-mortem fibre dissection study by Sachs published in 1892.

3. Future directions

Chapter 2 provides evidence that polysensory areas VIP and PIC+ are specialised for integration of optic flow and vestibular information regarding self-motion. This is in agreement with the previous findings that both VIP and PIC+ receive visual as well as vestibular information. Chapter 3 supports the findings that these two areas function as hubs for visuo-vestibular integration, by showing that the transmission of sensory information between these areas is enabled by structural connection through the white matter.

It should be noted, however, that there are at least two other cortical areas that might account for multisensory interaction underlying self-motion perception. One of these areas is MSTd, which is one of the optic-flow selective areas mentioned in this thesis. Because the work described in this thesis did not specifically identify MSTd, but instead localised the greater area in the proximity of MSTd (i.e. MT+), discussion of its potential role in visuo-vestibular

interaction based on the findings presented in this thesis is difficult. However, according to previous findings, MSTd responds to both visual and vestibular stimulation, and has been suggested to play a role in heading perception (Britten and van Wezel 1998; Fetsch et al. 2007). It is possible that this explains the differential activation to optic flow in the presence of illusory self-motion observed in MT+ (Chapter 2), but it is not conclusive until the same experiment is conducted and activity of MSTd and neighbouring areas is assessed separately.

The other candidate for a potential site of visuo-vestibular interaction is the superior temporal sulcus multisensory area (STSms). In monkeys, the homologue of STSms (i.e. the superior temporal polysensory area) has been shown to respond well to optic flow (Anderson and Siegel 1999). Although in humans, the responses of STSms to optic flow are somewhat elusive, STSms has been shown to respond to visual as well as vestibular stimulation (Smith et al. 2012), which places STSms in a good position to integrate visual and vestibular information for computation of self-motion. STSms is not discussed in the work presented in this thesis, because both studies described in this thesis employed the ROI approach and focused on the optic-flow selective areas based on the literature of optic-flow processing.

It is possible that all of these four polysensory areas are specialised for visuo-vestibular integration underlying self-motion perception. If this is the case, it is likely that these areas are specialised for different purposes (Smith et al. 2017). Future work should investigate the differential roles of these areas, interaction between them, and if and how they are structurally connected through the white matter.

In doing so, it is important to consider the "how." As noted in Chapter 1, advances in neuroimaging technology over the past three decades have been remarkable, and opened many

avenues to non-invasive studies of the living human brain. This means that it is now possible to examine the properties of cortical areas and the white matter tracts in relation to cognitive functions, as well as development and diseases. However, the rate at which those advances are made also means that researchers are required to adapt to the changes brought on by the advances. This requires developing new techniques to process and analyse the data acquired using the new imaging technology, understanding the advantages and disadvantages to one technique over others, selecting the most appropriate technique depending on the questions to be answered, combining multiple techniques if necessary.

Thus, future work should continue to employ the best-suited techniques to validate, strengthen and expand the literature. The next step in the investigation of the functional mechanism underlying integration of optic flow and vestibular information, will be to introduce multi-voxel pattern analysis (MVPA). Using MVPA instead of the standard univariate approach employed in Chapter 2 will allow for consideration of the patterns of response across multiple voxels simultaneously, and therefore increase the sensitivity to changes in cortical activity (Haxby et al. 2001; Arnoldussen et al. 2013). The results of MVPA would shed light on whether the patterns of response to optic flow accompanied by the sensation of self-motion are indeed different from those to the same stimulus but without the sensation of self-motion. For the investigation of the anatomical structure that supports the functional mechanisms, future work should be based on data of better quality. This will likely allow for extraction of a larger portion of shorter tracts that link the cortical sensory areas including SIPS; and for a more accurate estimation of the tracts' cortical endpoints, and therefore a more precise inference on the relations between the tracts and the cortical areas.

4. Conclusion

In conclusion, this thesis aimed to investigate the brain mechanism underlying perception of optic flow as a cue to self-motion. The fMRI experiment revealed that the polysensory areas VIP and PIC+ respond differentially to the same optic-flow stimulation when there is incongruence between the visual and vestibular input. This would suggest that, amongst the optic-flow selective areas, VIP and PIC+ are the loci of multisensory integration in the processing of optic flow, underlying perception of self-motion. The subsequent dMRI experiment in conjunction with tractography revealed that SIPS most likely supports the information transmission between the loci of visuo-vestibular integration via white matter. Taken together, these findings therefore provide a significant contribution to the literature by demonstrating the optic-flow selective areas specialised for integration of visual and vestibular cues to self-motion, the white matter connection between them, and leave unanswered questions to be addressed in future work.

References

Alais D, Burr D. 2004. The ventriloquist effect results from near-optimal bimodal integration. Curr Biol. 14:257-262.

Alexander DC, Barker GJ. 2005. Optimal imaging parameters for fiber-orientation estimation in diffusion MRI. Neuroimage. 27:357-367.

Andersen RA, Bracewell RM, Barash S, Gnadt JW, Fogassi L. 1990. Eye position effects on visual memory and saccade-related activity in areas LIP and 7a in the macaque. J Neurosci. 10:1176-1196.

Anderson KC, Siegel RM. 1999. Optic flow selectivity in the anterior superior temporal polysensoy area, STPa, of the behaving mokey. J Neurosci. 19:2681-2692.

Annese J, Gazzaniga MS, Toga AW. 2005. Localization of the human cortical visual area MT based on computer aided histological analysis. Cereb Cortex. 15:1044-1053.

Antal A, Baudewig J, Paulus W, Dechent P. 2008. The posterior cingulate cortex and planum temporale/parietal operculum are activated by coherent visual motion. Vis Neurosci. 25:17-26.

Arnoldussen DM, Goossens J, van den Berg AV. 2013. Differential responses in dorsal visual cortex to motion and disparity depth cues. Front Hum Neurosci. 7:815.

Baizer JS, Ungerleider LG, Desimone R. 1991. Organization of visual inputs to the inferior temporal and posterior parietal cortex in macaques. J Neurosci. 11:168-190.

Basser PJ, Pajevic S, Pierpaoli C, Duda J, Aldroubi A. 2000. In vivo fiber tractography using DT-MRI data. Magn Reson Med. 44:625-632.

Basser PJ, Pierpaoli C. 1996. Microstructural and physiological features of tissues elucidated by quantitative-diffusion-tensor MRI. J Magn Reson B. 111:209–219.

Bex PJ, Falkenberg HK. 2006. Resolution of complex motion detectors in the central and peripheral visual field. JOSA A. 23:1598-1607.

Bex PJ, Metha AB. Makous W. 1998. Psychophysical evidence for a functional hierarchy of motion processing mechanisms. JOSA A. 15:769-776.

Bex PJ, Metha AB. Makous W. 1999. Enhanced motion aftereffect for complex motions. Vis Res. 39:2229-2238.

Biagi L, Crespi SA, Tosetti M, Morrone MC. 2015. BOLD response selective to flow-motion in very young infants. PLoS Biol. 13:e1002260.

Bisley JW, Goldberg ME. 2003. Neuronal activity in the lateral intraparietal area and spatial attention. Science. 299:81-86.

Blanke O. 2012. Multisensory brain mechanisms of bodily self-consciousness. Nat Rev Neurosci. 13:556–571.

Blum JS, Chow KL, Pribram K. 1950. A behavioral analysis of the organisation of the parieo-temporo-preoccipital cortex. J Comp Neurol. 93:55-100.

Boussaoud D. Ungerleider LG, Desimone R. 1990. Pathways for motion analysis: cortical connections of the medial superior temporal and fundus of the superior temporal visual areas in the macaque. J Comp Neurol. 296:462-495.

Bullock TH, Bennett MV, Johnston D, Josephson R, Marder E, Fields RD. 2005. The neuron doctrine, redux. Science. 310:791-793.

Bürgel U, Amunts K, Hoemke L, Mohlberg H, Gilsbach JM, Zilles K. 2006. White matter fiber tracts of the human brain: three-dimensional mapping at microscopic resolution, topography and intersubject variability. Neuroimage. 29:1092-1105.

Burr DC, Santoro L. 2001. Temporal integration of optic flow, measured by contrast and coherence threshold. Vis Res. 41:1891-1899.

Butler JS, Smith ST, Campos JL, Bülthoff HH. 2010. Bayesian integration of visual and vestibular signals for heading. J Vis. 10:23.

Brandt T. 1999. Cortical visual-vestibular interaction for spatial orientation and self-motion perception. Curr Opin Neurol. 12:1-4.

Brandt T, Bartenstein P, Janek A, Dieterich M. 1998. Reciprocal inhibitory visual-vestibular interaction – visual motion stimulation deactivates the parieto-insular vestibular cortex. Brain. 121:1749-1758.

Brandt T, Dichgans J, Koenig E. 1972. Perception of self-rotation (circularvection) induced by optokinetic stimuli. Plügers Arch. 332:R98.

Brandt T, Dieterich M. 1999. The vestibular cortex: its locations, functions and disorders. Ann NY Acad Sci. 871:293-312.

Bremmer F, Schlack A, Ahah N, Zafiris O, Kubischik M, Hoffmann K-P, Zillies K, Fink G. 2001a. Polymodal motion processing in posterior parietal and premotor cortex: a human fMRI study strongly implies equivalencies between humans and monkeys. Neuron. 23:287-296.

Bremmer F, Schlack A, Fuhamel JR, Graf W, Fink GR. 2001b. Space coding in primate posterior parietal cortex. Neuroimage. 14:S46-S51.

Brewer AA, Press WA, Logothetis NK, Wandell BA. 2002. Visual areas in macaque cortex measured using functional magnetic resonance imaging. J Neurosci. 22:10416–10426.

Britten KH, Van Wezel RJA. 198. Electrical microstimulation of cortical area MST biases heading perception in monkeys. Nat Neurosci. 1:59-63.

Cabeza R, Ciaramelli E, Olson IR, Moscovitch M. 2008. The parietal cortex and episodic memory: an attentional account. Nat Rev Neurosci. 9:613-625.

Caiafa CF, Pestilli F. 2017. Multidimensional encoding of brain connectomes. bioRxiv. 107607.

Cardin V, Sherrington R, Hemsworth L, Smith AT. 2012. Human V6: functional characterisation and localisation. PLoS ONE. 7:e47685.

Cardin V, Smith AT. 2010. Sensitivity of human visual and vestibular cortical regions to egomotion-compatible visual stimulation. Cereb Cortex. 20:1964–1973.

Cardin V, Smith AT. 2011. Sensitivity of human visual cortical area V6 to stereoscopic depth gradients associated with self-motion. J Neurophysiol. 106:1240–1249.

Catani M, Allin MP, Husain M, Pugliese L, Mesulam MM, Murray RM, Jones DK. 2007. Symmetries in human brain language pathways correlate with verbal recall. Proc Natl Acad Sci USA. 104:17163-17168.

Catani M, Ffytche DH. 2005. The rises and falls of disconnection syndromes. Brain. 128:2224–2239.

Catani M, Howard RJ, Pajevic S, Jones DK. 2002. Virtual in vivo interactive dissection of white matter fasciculi in the human brain. Neuroimage. 17:77–94.

Catani M, Jones DK, Ffytche DH. 2005. Perisylvian language networks of the human brain. Ann Neurol. 57:8–16.

Catani M, Mesulam MM, Jakobsen E, Malik F, Martersteck A, Wieneke C, Thompson CK, Thiebaut de Schotten M, Dell'Acqua F, Weintraub S, Rogalski E. 2013. A novel frontal pathway underlies verbal fluency in primary progressive aphasia. Brain. 136:2619–2628.

Catani M, Thiebaut de Schotten M. 2012. Atlas of human brain connections. Oxford University Press.

Chen A, DeAngelis GC, Angelaki DE. 2011. Representation of vestibular and visual cues to self-motion in ventral intraparietal cortex. J Neurosci. 31:12036-12052.

Chun MM, Johnson MK. 2011. Memory: enduring traces of perceptual and reflective attention. Neuron. 72:520-535.

Corbetta M, Shulman GL. 2002. Control of goal-directed and stimulus-driven attention in the brain. Nat Rev Neurosci. 3:201–215.

Cottereau BR, Smith AT, Rima S, Fize D, Hejja-Brichard Y, Renaud L, Lejards C, Vayssiere N, Trotter Y, Durand J-B. 2017. Processing of egmotion-consistent optic flow in the rhesus macaque cortex. Cereb Cortex. 27:330-343.

Craddock RC, Jbabdi S, Yan CG, Vogelstein JT, Castellanos FX, Di Martino A, Kelly C, Heberlein K, Colcombe S, Milham MP. 2013. Imaging human connectomes at the macroscale. Nat Methods. 10:524–539.

Crowell JA, Banks MS. 1993. Perceiving heading with different retinal regions and types of optic flow. Percept Psychophys. 53:325-337.

Culham JC, Cavina-Pratesi CC, Singhal A. 2006. The role of parietal cortex in visuomotor control: what have we learned from neuroimaging? Neuropsychologia. 44:2668-2684.

Decety J, Lamm C. 2007. The role of the right temporoparietal junction in social interaction: how low-level computational processes contribute to meta-cognition. The Neuroscientist. 13:580-593.

Dell'Acqua F, Simmons A, Williams SC, Catani M. 2013. Can spherical deconvolution provide more information than fiber orientations? Hindrance modulated orientational anisotropy, a true-tract specific index to characterize white matter diffusion. Hum Brain Mapp. 34:2464-2483.

Deutschländer A, Bense S, Stephan T, Schwaiger M, Dieterich M, Brandt T. 2004. Rollvection versus linearvection: comparison of brain activations in PET. Hum Brain Mapp. 21:143–153.

Desikan RS, Ségonne F, Fischl B, Quinn BT, Dickerson BC, Blacker D, Buckner RL, Dale AM, Maguire RP, Hyman BT, Albert MS. 2006. An automated labeling system for

subdividing the human cerebral cortex on MRI scans into gyral based regions of interest. Neuroimage. 31: 968-980.

Dichgans J, Brandt T. 1978. “Visual-vestibular interaction: effects on self-motion perception and postual control” in Handbook of Sensory Physiology. Vol. 8. Eds R Held, HW Leibowitz, H-L Teuber. Berlin: Springer. 755-804.

Domini F, Caudek C. 1999. Perceiving surface slant from deformation of optic flow. J Exp Psychol Hum Percept Perform. 25:426-444.

Duan Y, Norcia AM, Yeatman JD, Mezer A. 2015. The structural properties of major white matter tracts in strabismic amblyopia. Invest Ophthalmol Vis Sci. 56:5152–5160.

Duffy DJ, Wurtz RH. 1991a. Sensitivity to MST neurons to optic flow stimuli. II. Mechanisms of response selectivity revealed by small-field stimuli. J Neurophysiol. 65:1346-1359.

Duffy DJ, Wurtz RH. 1991b. Sensitivity of MST neurons to optic flow stimuli. I. A contimuum of response selectivity to large-field stimuli. J Neurophysiol. 65:1329-1345.

Duffy DJ, Wurtz RH. 1995. Responses of monkey MST neuron to optic flow stimuli with shifted centres of motion. J Neurosci. 15:5192-5208.

Duhamel JR, Colby CL, Goldberg ME. 1998. Ventral intraparietal area of the macaque: visual and somatic response properties. J Neurophysiol. 79:126-136.

Dukelow SP, DeSouza JF, Culham JC, van den Berg AV, Menon RS, Vilis T. 2001. Distinguishing subregions of the human MT+ complex using visual fields and pursuit eye movements. J Neurophysiol. 86:1991-2000.

Dumoulin SO, Bittar RG, Kabani NJ, Baker CL Jr, Le Goualher G, Bruce Pike GB et al. 2000. A new anatomical landmark for the reliable identification of human area V5/MT: a quantitative analysis of sulcal patterning. Cereb Cortex. 10:454-463.

Dupont P, Orban GA, De Bruyn B, Verbruggen A, Mortelsmans L. 1994. Many areas in the human brain respond to visual motion. J Neurophysiol. 72:14201424.

Ernst MO, Banks MS. 2002. Humans integrate visual and haptic information in a statistically optimal fashion. Nature. 415:429-433.

Fan Q, Nummenmaa A, Witzel T, Zanzonico R, Keil B, Cauley S, Polimeni JR, Tisdall D, Van Dijk KR, Buckner RL, Wedeen VJ, Rosen BR, Wald LL. 2014. Investigating the capability to resolve complex white matter structures with high b-value diffusion magnetic resonance imaging on the MGH-USC Connectome scanner. Brain Connect. 4:718-726.

Fan Q, Witzel T, Nummenmaa A, Van Dijk KR, Van Horn JD, Drews MK, Somerville LH, Sheridan MA, Santillana RM, Snyder J, Hedden T, Shaw EE, Hollinshead MO, Renvall V, Zanzonico R, Keil B, Cauley S, Polimeni JR, Tisdall D, Buckner RL, Wedeen VJ, Wald LL, Toga AW, Rosen BR. 2016. MGH-USC Human Connectome Project datasets with ultra-high b-value diffusion MRI. Neuroimage. 124:1108-1114.

Felleman DJ, van Essen DC. 1991. Distributed hierarchical processing in the primate cerebral cortex. Cereb Cortex. 1:1-47.

Fetsch CR, Pouget A, DeAngelis GC, Angelaki DE. 2012. Neural correlates of reliability-based cue weighting during multisensory integration. Nat Neurosci. 15:146-154.

Fetsch CR, Turner AH, DeAngelis GC, Angelaki DE. 2009. Dynamic reweighting of visual and vestibular cues during self-motion perception. J Neurosci. 29:15601–15612.

Fields RD. 2008. White matter in learning, cognition and psychiatric disorders. Trends Neurosci. 31:361-370.

Fields RD. 2015. A new mechanism of nervous system plasticity: activity-dependent myelination. Nat Rev Neurosci. 16:756-767.

Fischer E, Bülthoff HH, Logothetis NK, Bartels A. 2012. Visual motion responses in the posterior cingulate sulcus: a comparison to V5/MT and MST. Cereb Cortex. 22:865-876.

Fischl B. 2012. FreeSurfer. Neuroimage. 62:774–781.

Forkel SJ, Mahmood S, Vergani F, Catani M. 2015. The white matter of the human cerebrum: part I The occipital lobe by Heinrich Sachs. Cortex. 62:182–202.

Frank LR. 2001. Anisotropy in high angular resolution diffusion-weighted MRI. Magn Reson Med. 45:935–939.

Frank SM, Baumann O, Mattingley JB, Greenlee MW. 2014. Vestibular and visual responses in human posterior insular cortex. J Neurophysiol. 112:2481–2491.

Frank SM, Greenlee MW. 2014. An MRI-compatible caloric stimulation device for the investigation of human vestibular cortex. J Neurosci Methods. 235:208–218.

Frank SM, Wirth AM, Greenlee MW. 2016 Visual-vestibular processing in the human sylvian fissure. J Neurophysiol. 10.1152/jn.00009.

Freeman TC, Harris MG, Meese TS. 1996. On the relationship between deformation and perceived surface slant. Vis Res. 36:317-322.

Friston KJ, Ashburner J. 2004. Generative and recognition models for neuroanatomy. Neuroimage. 23:21–24.

Furlan M, Wann JP, Smith AT. 2013. A representation of changing heading direction in human cortical areas pVIP and CSv. Cereb Cortex. 24:2848-2858.

Genç E, Bergmann J, Tong F, Blake R, Singer W, Kohler A. 2011. Callosal connections of primary visual cortex predict the spatial spreading of binocular rivalry across the visual hemifields. Front Hum Neurosci. 5.

Gibson JJ. 1950. The perception of the visual world. Boston: Houghton Mifflin.

Gibson JJ. 1954. The visual perception of objective motion and subjective movement. Psychol Rev. 61:304–314.

Giachritsis CD, Harris MG. 2005. Global versus local image expansion in estimating time-to-contact from complex optic flow. Perception. 34:577-585.

Goda N, Tachibana A, Okazawa G, Komatsu H. 2014. Representation of the material properties of objects in the visual cortex of nonhuman primates. J Neurosci. 34:2660–2673.

Gomez J, Pestilli F, Witthoft N, Golarai G, Liberman A, Poltoratski S, Yoon J, Grill-Spector K. 2015. Functionally defined white matter reveals segregated pathways in human ventral temporal cortex associated with category-specific processing. Neuron. 85:216–227.

Goossens J, Dukelow SP, Menon RS, Vilis T, van den Berg AV. 2006. Representation of head-centric flow in the human motion complex. J Neurosci. 26:5616-5627.

Graziano MS, Andersen RA, Snowden RJ. 1994. Tuning of MST neurons to spiral motions. J Neurosci. 14:54-67.

Greenberg AS, Verstynen T, Chiu YC, Yantis S, Schneider W, Behrmann M. 2012. Visuotopic cortical connectivity underlying attention revealed with white-matter tractography. J Neurosci. 32:2773–2782.

Greenlee MW, Frank SM, Kaliuzhna M, Blanke O, Bremmer F, Churan J, Cuturi LF, MacNeilage PR, Smith AT. 2016. Multisensory integration in self motion perception. Multisens Res. 29:525–556.

Gu Y, Watkins PV, DeAngelis GC, Angelaki DE. 2006. Visual and nonvisual contributions to three-dimensional heading selectivity in the medial superior temporal area. J Neurosci. 26:73-85.

Guevara M, Román C, Houenou J, Duclap D, Poupon C, Mangin JF, Guevara P. 2017. Reproducibility of superficial white matter tracts using diffusion-weighted imaging tractography. Neuroimage. 147:703-725.

Guldin WO, Grusser OJ. 1998. Is there a vestibular cortex? Trends Neruosci. 21:254-259.

Gurney KN, Wright MJ. 1996. A model for the spatial integration and differentiation of velocity signals. Vis Res. 36:2939-2955.

Hanada M, Ejima Y. 2000. Effects of roll and pitch components in retinal flow on heading judgement. Vis Res. 40:1827-1838.

Haxby JV, Gobbini ML, Furey ML, Ishai A. Schouten JL, Pietrini P. 2001. Distributed and overlapping representations of faces and objects in ventral temporal cortex. Science. 293:2425-2430.

Heuer HW, Britten KH. 2007. Linear responses to stochastic motion signals in area MST. J Neurophysiol. 98:1115-1124.

Holliday IE, Meese TS. 2008. Optic flow in human vision: MEG reveals a foveo-fugal bias in V1, specialization for spiral space in hMSTs, and global sensitivity in the IPS. J Vision. 8:1-24.

Honey CJ, Sporns O. 2008. Dynamical consequences of lesions in cortical networks. Hum Brain Mapp. 29:802–809.

Howard IP, Templeton WB. 1966. Human spatial orientation. Oxford: John Wiley & Sons.

Huk AC, Dougherty RF, Heeger DJ. 2002. Retinotopy and functional subdivision of human areas MT and MST. J Neurosci. 22:7195-7205.

Indovina I, Maffei V, Bosco G, Zago M, Macaluso E, Lacquaniti F. 2005. Representation of visual gravitational motion in the human vestibular cortex. Science. 308:416-419.

Jeurissen B, Tournier JD, Dhollander T, Connelly A, Sijbers J. 2014. Multi-tissue constrained spherical deconvolution for improved analysis of multi-shell diffusion MRI data. Neuroimage. 103: 411–426.

Jbabdi S, Lehman JF, Haber SN, Behrens TE. 2013. Human and monkey ventral prefrontal fibers use the same organizational principles to peach their targets: tracing versus tractography. J Neurosci. 33:3190–3201.

Kemerdere R, de Champfleur NM, Deverdun J, Cochereau J, Moritz-Gasser S, Herbet G, Duffau H. 2016. Role of the left frontal aslant tract in stuttering: a brain stimulation and tractographic study. J Neurol. 263:157-167.

Kennedy RS, Hettinger LJ, Harm DL, Ordy JM, Dunlap WP. 1996. Psychological scaling of circular vection (CV) produced by optokinetic (OKN) motion: individual differences and effects of practice. J Vestib Res. 6:331-341.

Kim M, Ducros M, Carlson T, Ronen I, He S, Ugurbil K, Kim D-S. 2006. Anatomical correlates of the functional organization in the human occipitotemporal cortex. Magn Reson Imaging. 24:583–590.

Kinoshita M, de Champfleur NM, Deverdun J, Moritz-Gasser S, Herbet G, Duffau H. 2015. Role of fronto-striatal tract and frontal aslant tract in movement and speech: an axonal mapping study. Brain Struc and Func. 220:3399-3412.

Klam F, Graf W. 2003. Vestibular response kinematics in posterior parietal cortex neurons of macaque monkeys. Eur J Neurosci. 18:995-1010.

Kleinschmidt A, Thilo KV, Büchel C, Gresty MA, Bronstein AM, Frackowiak RSJ. 2002. Neural correlates of visual-motion perception as object- or self-motion. Neuroimage. 16:873–882.

Knill DC, Saunders JA. 2003. Do humans optimally integrate stereo and texture information for judgements of surface slant? Vis Res. 43:2539-2558.

Koenderink JJ. 1986. Optic flow. Vison Res. 26:161-179.

Koenderink JJ, van Doorn AJ. 1975. Invariant properties of the motion parallax field due to the movement of rigid bodies relative to an observer. Optica Acta. 22:773-791.

Koenigs M, Barbey AK, Postle BR, Grafman J. 2009. Superior parietal cortex is critical for the manipulation of information in working memory. J Neurosci. 29:14980-14986.

Kolster H, Janssens T, Orban GA, Vanduffel W. 2014. The retinotopic organization of macaque occipitotemporal cortex anterior to V4 and caudoventral to the middle temporal (MT) cluster. J Neurosci. 34:10168–10191.

Kovács G, Raabe M, Greenlee MW. 2008. Neural correlates of visually induced self-motion illusion in depth. Cereb Cortex. 18:1779–1787.

Kronfeld-Duenias V, Amir O, Ezrati-Vinacour R, Civier O, Ben-Shachar M. 2016. The frontal aslant tract underlies speech fluency in persistent developmental stuttering. Brain Struc Func. 221:365-381.

Lappe M, bremmer F, van den berg AV. 1999. Perception of self-motion from visual flow. Trends Cogn Sci. 3:329-226.

Lebel C, Gee M, Camicioli R, Wieler M, Martin W, Beaulieu C. 2012. Diffusion tensor imaging of white matter tract evolution over the lifespan. Neuroimage. 60:340–352.

Lee DN. 1980. The optic flow field: the foundation of vision. Philos Trans R Soc Lond B Biol Sci. 290:169-179.

Lee DN, Aronson E. 1974. Visual proprioceptive control of standing in human infants. Percept Psychophys. 15:529-532.

Lee Masson H, Wallraven C, Petit L. 2017. “Can touch this”: cross-modal shape categorization performance is associated with microstructural characteristics of white matter association pathways. Hum Brain Mapp. 38:842-854.

Leichnetz GR. 2001. Connections of the medial posterior parietal cortex (areas 7m) in the monkey. Anat Rec. 263:215-236.

Leong JK, Pestilli F, Wu CC, Samanez-Larkin GR, Knutson B. 2016. White-matter tract connecting anterior insula to nucleus accumbens correlates with reduced preference for positively skewed gambles. Neuron. 89:63–69.

Lewis JW, van Essen DC. 2000. Corticocortical connections of visual sensorimotor and multimodal processing areas in the parietal lobe of the macaque monkey. J Comp Neurol. 428:112-137.

Logan DJ, Duffy CJ. 2006. Cortical area MSTd combines visual cues to represent 3-D self-movement. Cereb Cortex. 16:1494-1507.

Longuet-Higgins HC, Prazdny K. 1980. The interpretation of a moving retinal image. Philos Trans R Soc Lond B Biol Sci. 208:385-397.

Malania M, Konrad J, Jägle H, Werner JS, Greenlee MW. 2017. Compromised integrity of central visual pathways in patients with macular degeneration. Invest Ophthalmol Vis Sci. 58:2939-2947.

Mars RB, Foxley S, Verhagen L, Jbabdi S, Sallet J, Noonan MP, Neubert F-X, Andersson JL, Croxson PL, Dunbar RIM, Khrapitchev AA, Sibson NR, Miller KL, Rushworth MFS. 2015. The extreme capsule fiber complex in humans and macaque monkeys: a comparative diffusion MRI tractography study. Brain Struct Funct. [Epub ahead of print].

Matsumoto R, Ikeda A, Nagamine T, Matsuhashi M, Ohara S, Yamamoto J et al. 2004. Subregions of human MT complex revealed by comparative MEG and direct electrocorticographic recordings. Clin Neurophysiol. 115:2056-2065.

Maunsell JH, van Essen DC. 1983. Functional properties of neurons in the middle temporal visual area of the macaque monkey. I. Selectivity for stimulus direction, speed, and orientation. J Neurophysiol. 49:1127-1147.

Meese TS, Anderson SJ. 2002. Spiral mechanisms are required to account for summation of complex motion components. Vis Res. 42:1073-1080.

Meese TS, Harris MG. 1997. Computation of surface slant from optic flow: orthogonal components of speed gradient can be combined. Vis Res. 37:2369-2379.

Meese TS, Harris MG. 2001a. Broad direction bandwidths for complex motion mechanisms. Vis Res. 41:1901-1914.

Meese TS, Harris MG. 2001b. Independent detectors for expansion and rotation, and for orthogonal components of deformation. Perception. 30:1189-1202.

Meese TS, Harris MG, Freeman TC. 1995. Speed gradients and the perception of surface slant: analysis is two-dimensional not one-dimensional. Vis Res. 35:2879-2888.

Mezer A, Yeatman JD, Stikov N, Kay KN, Cho NJ, Dougherty RF, Perry ML, Parvizi J, Hua LH, Butts-Pauly K, Wandell BA. 2013. Quantifying the local tissue volume and composition in individual brains with magnetic resonance imaging. Nature Med. 19:1667-1672.

Mohammadi S, Carey D, Dick F, Diedrichsen J, Sereno MI, Reisert M, Callaghan MF, Weiskopf N. 2015. Whole-brain in-vivo measurements of the axonal g-ratio in a group of 37 healthy volunteers. Front Neurosci. 9:441.

Mori S, Zhang J. 2006. Principles of diffusion tensor imaging and its applications to basic neuroscience research. Neuron. 51:527–539.

Morrone MC, Burr DC, Di Pietro S, Stefanelli MA. 1999. Cardinal directions for visual optic flow. Curr Biol. 9:763-766.

Morrone MC, Burr DC, Vaina LM. 1995. Two stages of visual processing for radial and circular motion. Nature. 376:507-509.

Morrone MC, Tosetti M, Montanaro D, Fiorentini A, Cioni G, Burr DC. 2000. A cortical area that responds specifically to optic flow revealed by fMRI. Nat Neurosci. 3:1322-1328.

Nishiike S, Nakagawa S, Nakagawa A, Uno A, Tonoike M, Takeda N, Kubo T. 2002. Magnetic cortical responses evoked by visual linear forward acceleration. Neuroreport. 13:1805-1808.

Ogawa S, Lee TM, Kay AR, Tank DW. 1990. Brain magnetic resonance imaging with contrast dependent on blood oxygenation. Proc Natl Acad Sci USA. 87: 9868-9872.

Ogawa S, Takemura H, Horiguchi H, Terao M, Haji T, Pestilli F, Yeatman JD, Tsuneoka H, Wandell BA, Masuda Y. 2014. White matter consequences of retinal receptor and ganglion cell damage. Invest Ophthalmol Vis Sci. 55:6976–6986.

Oishi K, Huang H, Yoshioka T, Ying SH, Zee DS, Zilles K, Amunts K, Woods R, Toga AT, Pike GB, Rosa-Neto P, Evans AC, van Zijl PCM, Mazziotta JC, Mori S. 2011. Superficially located white matter structures commonly seen in the human and the macaque brain with diffusion tensor imaging. Brain Connect. 1:37-47.

Oishi K, Zilles K, Amunts K, Faria A, Jiang H, Li X, Akhter K, Hua K, Woods R, Toga AW, Bruce Pike G, Rosa-Neto P, Evans A, Zhang J, Huang H, Miller MI, van Zijl PCM, Mazziotta J, Mori S. 2008. Human brain white matter atlas: identification and assignment of common anatomical structures in superficial white matter. Neuroimage. 43: 447-457.

Pajevic S, Pierpaoli C. 1999. Color schemes to represent the orientation of anisotropic tissues from diffusion tensor data: application to white matter fiber tract mapping in the human brain. Magn Reson Med. 42:526–540.

Pestilli F, Yeatman JD, Rokem A, Kay KN, Wandell BA. 2014. Evaluation and statistical inference for human connectomes. Nat Methods. 11:1058–1063.

Pitzalis S, Galleti C, Huang R-S, Patria F, Committeri G, Galati G et al. 2006. Wide-field retinotopy defines human cortical visual area V6. J Neurosci. 26:7962-7973.

Pitzalis S, Sereno MI, Committeri G, Fattori P, Galati G, Patria F, Galletti C. 2010. Human v6: the medial motion area. Cereb Cortex. 20:411–424.

Platt ML, Glimcher PW. 1999. Neural correlates of decision variables in parietal cortex. Nature. 400:233-238.

Prsa M, Gale S, Blanke O. 2012. Self-motion leads to mandatory cue fusion across sensory modalities. J Neurophysiol. 108: 2282-2291.

Prsa M, Jimenez-Rezende D, Blanke O. 2015. Inference of perceptual priors from path dynamics of passive self-motion. J Neurophysiol. 113:1400–1413.

Redlick FP, Jenkin M, Harris LJ. 2001. Humans can use optic flow to estimate distance of travel. Vis Res. 41:213-219.

Reveley C, Seth AK, Pierpaoli C, Silva AC, Yu D, Saunders RC, Leopold DA, Ye FQ. 2015. Superficial white matter fiber systems impede detection of long-range cortical connections in diffusion MR tractography. Proc Natl Acad Sci USA. 112:E2820–E2828.

Rilling JK, Glasser MF, Preuss TM, Ma X, Zhao T, Hu X, Behrens TEJ. 2008. The evolution of the arcuate fasciculus revealed with comparative DTI. Nat Neurosci. 11:426–428.

Rizzolatti G, Luppino G. 2001. The cortical motor system. Neuron. 31:889-901.

Rohde GK, Barnett AS, Basser PJ, Marenco S, Pierpaoli C. 2004. Comprehensive approach for correction of motion and distortion in diffusion-weighted MRI. Magn Reson Med. 51:103–114.

Rokem A, Takemura H, Bock A, Scherf KS, Behrmann M, Wandell B, Fine I, Bridge H, Pestilli F. 2017. The visual white matter: the application of diffusion MRI and fiber tractography to vision science. J Vis. 17:4, 1-30.

Rokem A, Yeatman JD, Pestilli F, Kay KN, Mezer A, van der Walt S, Wandell BA. 2015. Evaluating the accuracy of diffusion MRI models in white matter. PLoS One. 10:e0123272.

Royden CS, Banks MS, Crowell JA. 1992. The perception of heading during eye movements. Nature. 360:583-585.

Royden CS, Picone LJ. 2007. A model for simultaneous computation of heading and depth in the presence of rotations. Vis Res. 47:3025-3040.

Sachs H. 1892. Das Hemisphärenmark des menschlichen Grosshirns. Leipzig: Verlag von Georg Thieme.

Saito H-A, Yukie M, Tanaka K, Hikosaka K, Fukuda Y, Iwai E. 1986. Integration of direction signals of image motion in the superior temporal sulcus of the macaque monkey. J Neurosci. 6:145-157.

Schlack A, Hoffmann KP, Bremmer F. 2002. Interaction of linear vestibular and visual stimulation in the macaque ventral intraparietal area (VIP). Eur J Neurosci. 16:1877-1886.

Schaafsma SJ, Duysens J. 1996. Neurons in the ventral intraparietal are of awake macaque monkey closely resemble neurons in the dorsal part of the medial superior temporal area in their responses to optic flow patterns. J Neurophysiol. 76:4056-4068.

Schmahmann JD, Pandya D. 2006. Fiber Pathways of the Brain. New York: Oxford Univ Press.

Schmahmann JD, Pandya DN, Wang R, Dai G, D'Arceuil HE, de Crespigny AJ, Wedeen VJ. 2007. Association fibre pathways of the brain: parallel observations from diffusion spectrum imaging and autoradiography. Brain. 130:630–653.

Smith AT, Beer AL, Furlan M, Mars RB. 2017. Connectivity of the cingulate sulcus visual area (CSv) in the human cerebral cortex. Cereb Cortex. 1-13.

Smith AT, Greenlee MW, DeAngelis GC, Angelaki DE. 2017. Distributed visual-vestibular processing in the cerebral cortex of man and macaque. Multisens Res. 30:91-120.

Smith RE, Tournier JD, Calamante F, Connelly A. 2012. Anatomically-constrained tractography: improved diffusion MRI streamlines tractography through effective use of anatomical information. Neuroimage. 62:1924-1938.

Smith AT, Wall MB, Thilo KV. 2012. Vestibular inputs to human motion-sensitive visual cortex. Cereb Cortex. 22:1068–1077.

Smith AT, Wall MB, Williams AL, Singh KD. 2006. Sensitivity to optic flow in human cortical areas MT and MST. Eur J Neurosci. 23:561-569.

Snowden RJ, Milne AB. 1996. The effects of adapting to complex motions: position invariance and tuning to spiral motions. J Cogn Neurosci. 8:435-452.

Snowden RJ, Milne AB. 1997. Phantom motion aftereffects: evidence of detectors for the analysis of optic flow. Curr Biol. 7:717-722.

Sotiropoulos SN, Jbabdi S, Xu J, Andersson JL, Moeller S, Auerbach EJ, Glasser MF, Hernandez M, Sapiro G, Jenkinson M, Feinberg DA, Yacoub E, Lenglet C, Van Essen DC, Ugurbil K, Behrens TE, Consortium, W. U-Minn HCP. 2013. Advances in diffusion MRI acquisition and processing in the Human Connectome Project. Neuroimage. 80:125–143.

Stikov N, Campbell JS, Stroh T, Lavelée M, Frey S, Novek J, Naura S, Ho MK, Bedell BJ, Dougherty RF, Leppert IR, Boudreau M, Narayanan S, Duval T, Cohen-Adad J, Picard PA. Gasecka A, Cote D, Bruce Pike G. 2015. In vivo histology of the myelin g-ratio with magnetic resonance imaging. Neuroimage. 118:397-405.

Tanaka K, Saito H. 1989. Analysis of motion of the visual field by direction, expansion/contraction, and rotation cells clustered in the dorsal part of the medial superior temporal area of the macaque monkey. J Neurophysiol. 62:626-641.

Takemura H, Caiafa CF, Wandell BA, Pestilli F. 2016. The ensemble tractography. PLoS Comput Biol. 12:e1004692.

Takemura H, Pestilli F, Weiner KS, Keliris GA, Landi SM, Sliwa J, Ye FQ, Barnett MA, Leopold DA, Freiwald WA, Logothetis NK, Wandell BA. 2017. Occipital white matter tracts in human and macaque. Cereb Cortex. 27:3346–3359.

Takemura H, Rokem A, Winawer J, Yeatman JD, Wandell BA, Pestilli F. 2016. A major human white-matter pathway between dorsal and ventral visual cortex. Cereb Cortex. 26:2205–2214.

Tavor I, Yablonski M, Mezer A, Rom S, Assaf Y, Yovel G. 2014. Separate parts of occipito-temporal white matter fibers are associated with recognition of faces and places. Neuroimage. 86:123-130.

Thiebaut de Schotten M, Dell'Acqua F, Forkel SJ, Simmons A, Vergani F, Murphy DG, Catani M. 2011. A lateralized brain network for visuospatial attention. Nat Neurosci. 14:1245–1246.

Thiebaut de Schotten M, Dell'Acqua F, Valabregue R, Catani M. 2012. Monkey to human comparative anatomy of the frontal lobe association tracts. Cortex. 48:82-96.

Thiebaut de Schotten MT, Kinkingnehun S, Delmaire C, Lehericy S, Duffau H, Thivard L, Volle E, Levy R, Dubois B, Bartolomeo P. 2008. Visualization of disconnection syndromes in humans. Cortex. 44:1097-1103.

Tournier JD, Calamante F, Connelly A. 2007. Robust determination of the fibre orientation distribution in diffusion MRI: non-negativity constrained super-resolved spherical deconvolution. Neuroimage. 35:1459–1472.

Tournier JD, Calamante F, Connelly A. 2012. MRtrix: diffusion tractography in crossing fiber regions. Int J Imaging Syst Technol. 22:53–66.

Tsao DY, Moeller S, Freiwald WA. 2008. Comparing face patch systems in macaques and humans. Proc Natl Acad Sci USA. 105:19514–19519.

Tsao DY, Vanduffel W, Sasaki Y, Fize D, Knutsen TA, Mandeville JB, Wald LL, Dale AM, Rosen BR, Van Essen DC, Livingstone MS, Orban GA, Tootell RB. 2003. Stereopsis activates V3A and caudal intraparietal areas in macaques and humans. Neuron. 39:555–568.

Uesaki M, Takemura H, Ashida H. 2018. Computational neuroanatomy of human stratum proprium of interparietal sulcus. Brain Struct Funct. 223:489.

Uesaki M, Ashida H. 2015. Optic-flow selective cortical sensory regions associated with self-reported states of vection. Front Psychol. 6:775.

Uncapher MR, Wagner AD. 2009. Posterior parietal cortex and episodic encoding: insights from fMRI subsequent memory effects and dual-attention theory. Neurobiol Learn Mem. 91:139–154.

Ungerleider LG, Desimone R. 1986. Cortical connections of visual area MT in the macaque. J Comp Neurol. 248:190-222.

Van Essen DC, Smith SM, Barch DM, Behrens TE, Yacoub E, Ugurbil K, Consortium, W. U-Minn HCP. 2013. The WU-Minn Human Connectome Project: an overview. Neuroimage. 80:62–79.

Vergani F, Mahmood S, Morris CM, Mitchell P, Forkel SJ. 2014. Intralobar fibres of the occipital lobe: a post mortem dissection study. Cortex. 56:145–156.

Wada A, Sakano Y, Ando H. 2016. Differential responses to a visual self-motion signal in human medial cortical regions revealed by wide-view stimulation. Front Psychol. 7:309.

Wade A, Augath M, Logothetis N, Wandell B. 2008. fMRI measurements of color in macaque and human. J Vis. 8:6 1–19.

Wakana S, Jiang H, Nagae-Poetscher LM, van Zijl PC, Mori S. 2004. Fiber tract-based atlas of human white matter anatomy. Radiology. 230:77–87.

Wall MB, Smith AT. 2008. The representation of egomotion in the human brain. Curr Biol. 18:191–194.

Wandell BA. 2016. Clarifying Human White Matter. Annu Rev Neurosci. 39:103–128.

Wandell BA, Yeatman JD. 2013. Biological development of reading circuits. Curr Opin Neurobiol. 23:261-268.

Warren WH Jr, Hannon DJ. 1988. Direction of self-motion is perceived from optical flow. Nature. 336:162–163.

Warren PA, Rushton SK. 2009. Optic flow processing for the assessment of object movement during ego movement. Curr Biol. 19:1555-1560.

Wedeen VJ, Rosene DL, Wang R, Dai G, Mortazavi F, Hagmann P, Kaas JH, Tseng WY. 2012. The geometric structure of the brain fiber pathways. Science. 335:1628–1634.

Weiner KS, Yeatman JD, Wandell BA. 2016. The posterior arcuate fasciculus and the vertical occipital fasciculus. Cortex. [Epub ahead of print]

Weiskopf N, Mohammadi S, Lutti A, Callaghan MF. 2015. Advances in MRI-based computational neuroanatomy: from morphometry to in-vivo histology. Curr Opin Neurol. 28:313-322.

Wertheim A. 1994. Motion perception during self-motion – the direct versus inferential controversy revisited. Behav Brain Sci. 17:293-311.

Wexler M, Panerai F, Lamouret I, Droulez J. 2001. Self-motion and the perception of stationary objects. Nature. 409:85-88.

Wiest G, Zimprich F, Prayer D, Czech T, Serles W, Baumgartner C. 2004. Vestibular processing in human paramedian precuneus as shown by electrical cortical stimulation. Neurology. 62:473–475.

Yantis S, Schwarzbach J, Serences JT, Carlson RL, Steinmetz MA, Pekar JJ, Courtney SM. 2002. Transient neural activity in human parietal cortex during spatial attention shifts. Nat Neurosci. 5:995-1002.

Yeatman JD, Dougherty RF, Ben-Shachar M, Wandell BA. 2012. Development of white matter and reading skills. Proc Natl Acad Sci USA. 109:E3045–E3053.

Yeatman JD, Dougherty RF, Myall NJ, Wandell BA, Feldman HM. 2012. Tract profiles of white matter properties: automating fiber-tract quantification. PLoS One. 7:e49790.

Yeatman JD, Dougherty RF, Rykhlevskaia E, Sherbondy AJ, Deutsch GK, Wandell BA, Ben-Shachar M. 2011. Anatomical properties of the arcuate fasciculus predict phonological and reading skills in children. J Cogn Neurosci. 23:3304–3317.

Yeatman JD, Rauschecker AM, Wandell BA. 2013. Anatomy of the visual word form area: adjacent cortical circuits and long-range white matter connections. Brain Lang. 125:146–155.

Yeatman JD, Wandell BA, Mezer AA. 2014. Lifespan maturation and degeneration of human brain white matter. Nat Commun. 5:4932.

Yeatman JD, Weiner KS, Pestilli F, Rokem A, Mezer A, Wandell BA. 2014. The vertical occipital fasciculus: a century of controversy resolved by in vivo measurements. Proc Natl Acad Sci USA. 111:E5214–E5223.

Yushkevich PA, Piven J, Hazlett HC, Smith RG, Ho S, Gee JC, Gerig G. 2006. User-guided 3D active contour segmentation of anatomical structures: significantly improved efficiency and reliability. Neuroimage. 31:1116–1128.

Zhang H, Schneider T, Wheeler-Kingshott CA, Alexander DC. 2012. NODDI: practical in vivo neurite orientation dispersion and density imaging of the human brain. Neuroimage. 61:1000-1016.

Zhang Y, Zhang J, Oishi K, Faria AV, Jiang H, Li X, Akhter K, Rosa-Neto P, Pike GB, Evans A, Toga AW, Woods R, Mazziotta JC, Miller MI, van Zijl PCM, Mori S. 2010. Atlas-guided tract reconstruction for automated and comprehensive examination of the white matter anatomy. Neuroimage. 52:1289-1301.

Zhong H, Cornilleau-Peres V, Cheong LF, Yeow GM, Droulez J. 2006. The visual perception of plane tilt from motion in small field and large field: psychophysics and theory. Vis Res. 46:3494-3513.